JOURNAL OF PETROLOGY | VOLUME 49 | NUMBER 7 | PAGES 1397–1426 | 2008 | doi:10.1093/petrology/egn030

Dynamic Magma Systems, Crustal Recycling, and Alteration in the Central Sierra Nevada Batholith: the Oxygen Isotope Record

JADE STAR LACKEY[1]*, JOHN W. VALLEY[2], JAMES H. CHEN[3] AND DANIEL F. STOCKLI[4]

[1]GEOLOGY DEPARTMENT, POMONA COLLEGE, CLAREMONT, CA 91711, USA

[2]DEPARTMENT OF GEOLOGY AND GEOPHYSICS, UNIVERSITY OF WISCONSIN, MADISON, WI 53706, USA

[3]SCIENCE DIVISION, JET PROPULSION LABORATORY, CALIFORNIA INSTITUTE OF TECHNOLOGY, PASADENA, CA 91109, USA

[4]DEPARTMENT OF GEOLOGY, UNIVERSITY OF KANSAS, LAWRENCE, KS 66045, USA

RECEIVED JANUARY 6, 2007; ACCEPTED MAY 27, 2008
ADVANCE ACCESS PUBLICATION JUNE 19, 2008

Values of $\delta^{18}O$ of zircon from the central Sierra Nevada batholith (SNB), California, yield fresh insight into the magmatic evolution and alteration history of this classic convergent margin batholith. Direct comparison of whole-rock and zircon (Zrc) $\delta^{18}O$ provides evidence for modest (0.5‰), but widespread, alteration, which has complicated interpretation in previous whole-rock $\delta^{18}O$ studies. Four discrete belts of $\delta^{18}O$ values are recognized in the central Sierra. A small belt of plutons with relatively low $\delta^{18}O$(Zrc) values (5·2–6·0‰) intrudes the foothills, with a sharp increase of $\delta^{18}O$ revealing the concealed Foothills Suture; high $\delta^{18}O$(Zrc) values (7·0–8·5‰) dominate the rest of the western SNB. East of the axis of the Sierra, $\delta^{18}O$ is distinctly lower (6·75–5·75‰), and decreases monotonically to the Sierra Crest. A sharp 1‰ increase of $\delta^{18}O$ in the eastern Sierra reveals a second crustal boundary, with the fourth belt hosted in high-$\delta^{18}O$ North American crust in the White Mountains and Owens and Long Valleys. Correlated O, Sr, and Pb isotope ratios reveal differences in magma generation between the western and eastern Sierra. The western Sierra experienced massive crustal recycling, with substantial melting and mobilization of accreted oceanic and volcanic arc rocks; crustal contamination affects many western SNB plutons. In contrast, the eastern Sierra was dominated by voluminous recycling of the lithospheric mantle and lower crust, with minimal crustal contamination. Batholith-wide shifts in $\delta^{18}O$ occur between pulses of Cretaceous magmatism that may be linked to tectonic reorganizations of magma sources. Within intrusive suites, $\delta^{18}O$ may be unchanged (Tuolumne); increase (Sonora and Whitney); or decrease (Sequoia and John Muir) with time. These trends show stable long-lived sources, or those where recycling and contamination may increase or decrease with time. Overall, $\delta^{18}O$ reveals diverse magma system behavior at a range of scales in the Sierran arc.

KEY WORDS: *zircon; crustal growth; granitoids; supracrustal; magma systems; Sierra Nevada*

INTRODUCTION

The Sierra Nevada batholith (SNB, Fig. 1) has been intensely studied for decades to deduce the petrogenesis of individual plutons and intrusive suites and to understand the integrated history of the arc that formed it (see Bateman, 1992; Moore, 2000). Isotope studies have been particularly helpful in identifying significant crustal and mantle 'reservoirs' that contributed to the diversity of magmas of the SNB (Doe & Delevaux, 1973; Kistler & Peterman, 1973, 1978; DePaolo, 1980, 1981; Masi *et al.*, 1981; Saleeby *et al.*, 1987; Kistler, 1990; Kistler & Ross, 1990; Chen & Tilton, 1991; Kistler & Fleck, 1994; Lee *et al.*, 2000; Ducea, 2001; Ratajeski *et al.*, 2001; Wenner & Coleman, 2004; Lackey *et al.*, 2005, 2006). Reservoirs include sub-arc mantle, subducted ocean crust, Phanerozoic sedimentary rocks, and

*Corresponding author. Telephone: (909) 621-8677. Fax: (909) 621-8552. E-mail: JadeStar.Lackey@pomona.edu

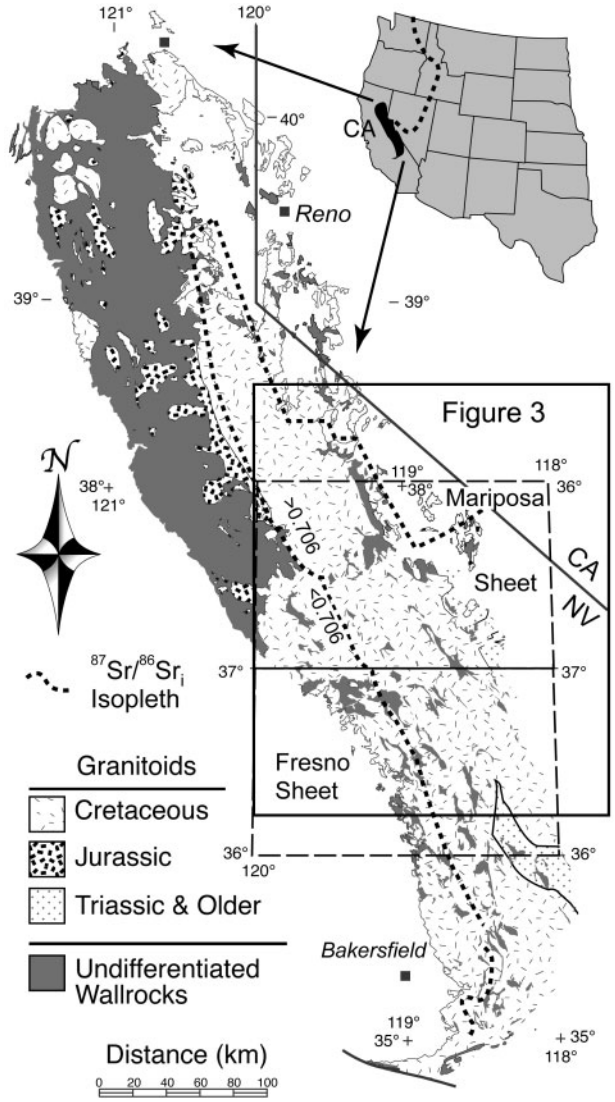

Fig. 1. Generalized geological map of the Sierra Nevada batholith. Study area (Fig. 3) is denoted by solid box, with Mariposa and Fresno $1^\circ \times 2^\circ$ map sheets for reference. The initial $^{87}Sr/^{86}Sr = 0{\cdot}706$ line of Kistler (1990) is shown as a dashed line. Map after Jennings *et al.* (1977), Moore & Sisson (1987), Ross (1987), Saleeby *et al.* (1987), Bateman (1992), and Moore (2000).

Precambrian continental crust. The relative contributions of these reservoirs to SNB magmas are largely unknown. For example, studies of mantle xenoliths show considerable geochemical heterogeneity in the sub-arc mantle (Mukhopadhyay & Manton, 1994; Ducea, 1998, 2001, 2002; Lee *et al.*, 2000), which suggests that the lithospheric mantle was heavily contaminated during subduction in the Jurassic and Triassic. Also, the amount of recycling of young rocks in the arc is uncertain. Recent experimental studies have reproduced characteristic major and trace element patterns of SNB granitoids by partially melting gabbroic compositions at pressure, temperature, and fluid conditions inferred for the magma-generating regions of the arc (Ratajeski *et al.*, 2005; Sisson *et al.*, 2005). These findings suggest significant remelting of mantle-derived basaltic sources at the base of the arc.

Oxygen isotopes are well suited to clarifying ambiguity of magma source and contamination processes in the SNB. Low-temperature fractionation of $^{18}O/^{16}O$, especially in the presence of water, imparts unambiguous $\delta^{18}O$ 'supracrustal' signatures in sedimentary rocks that form at the Earth's surface, or in igneous and metamorphic rocks that are hydrothermally altered there. When such rocks melt following subduction or burial, the $\delta^{18}O$ of these melts contrasts markedly with the restricted $\delta^{18}O$ range of the primitive mantle ($5{\cdot}7 \pm 0{\cdot}3‰$; Taylor & Sheppard, 1986).

Despite the utility of oxygen isotopes, their application to study the SNB has long been regarded with skepticism. Masi *et al.* (1981) conducted the first large-scale oxygen isotope study of the SNB. They found that, unlike the coeval Peninsular Ranges batholith (Fig. 2a; Taylor & Silver, 1978; Silver *et al.*, 1979), the variation of $\delta^{18}O$ with Sr_i in the SNB did not define a simple binary mixing pattern. Subsequent studies have shown an increasingly complex data array (Fig. 2b). Furthermore, hydrogen isotope analyses have revealed low δD values, -85 and lower, indicating hydrothermal alteration of many samples.

Our study provides fresh insight into the origin and evolution of magmas in the SNB. We present a comprehensive laser fluorination study of $\delta^{18}O$ of zircon (Zrc) in the central Sierra (Fig. 3). Zircon was selected for the study because it is highly retentive of magmatic $\delta^{18}O$ (Valley, 2003; Page *et al.*, 2007). Prior study showed that analysis of $\delta^{18}O$(Zrc) in the SNB resolves magmatic $\delta^{18}O$ in rocks that have undergone subsolidus exchange and hydrothermal alteration (Lackey *et al.*, 2001, 2003, 2005, 2006). In this study, over 100 rocks were analyzed for both $\delta^{18}O$(WR) (where WR is whole-rock) and $\delta^{18}O$(Zrc); direct comparison of $\delta^{18}O$ is presented to illustrate the magnitude and frequency of alteration of $\delta^{18}O$(WR). Also, we detail how whole-rock SiO_2 content and $\delta^{18}O$(Zrc) allow calculation of magmatic $\delta^{18}O$(WR). These findings elucidate the scale and nature of magma systems in the arc.

GEOLOGICAL BACKGROUND

The central Sierra Nevada batholith is a collage of plutons and intrusive suites (Fig. 3) with pronounced spatial variation in composition, age, and isotope chemistry. Cretaceous granitoids are exposed over *c.* 35 000 km^2 (Fig. 1). The estimated original thickness of granitic crust in the batholith is 35 km (Fliedner *et al.*, 2000; Saleeby *et al.*, 2003); thus the Sierran arc must have generated at least 1×10^6 km^3 of granitic magma between 120 and 85 Myr ago. The batholith has long been recognized to have lateral (west to east) gradients in bulk composition (Moore, 1959; Bateman, 1992), pluton age (Kistler & Peterman, 1973, 1978;

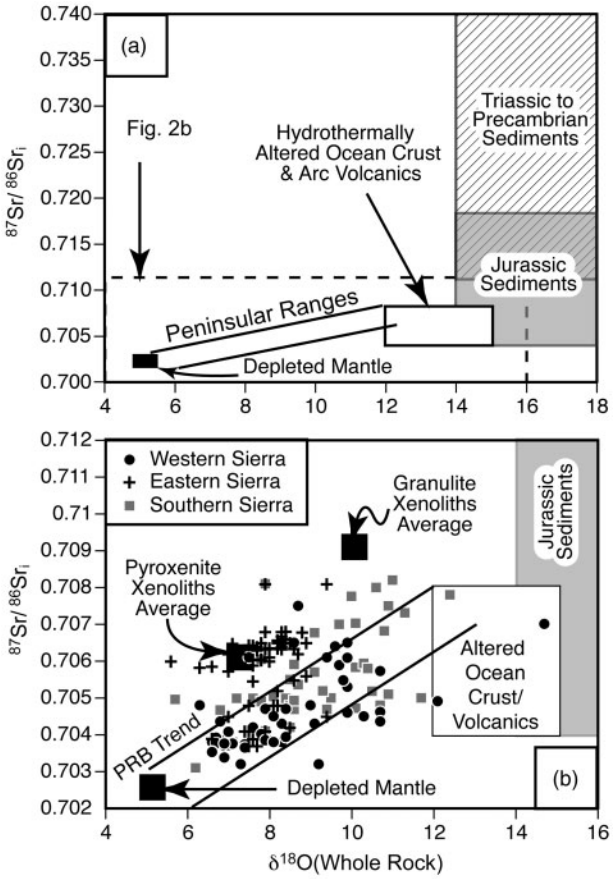

Fig. 2. Oxygen and strontium isotopes in the Sierra Nevada and Peninsular Ranges batholiths. (a) The Peninsular Ranges trend relative to recognized reservoirs. (b) Sierran isotopic values by geographical area. Sources include: xenoliths (Ducea, 1998); altered ocean crust (McCulloch *et al.*, 1980); altered greywacke (Magaritz & Taylor, 1976); Sierran metamorphic wall-rocks (Kistler & Peterman, 1973; DePaolo, 1981; Ross, 1983a, 1983b; Zeng *et al.*, 2005). Data in (b) from Taylor & Silver (1978), Masi *et al.* (1981), Saleeby *et al.* (1987), Clemens-Knott (1992), Kistler (1993), Kistler & Fleck (1994), and Truschel (1996).

Stern *et al.*, 1981; Chen & Moore, 1982), major and trace element geochemistry (Ague & Brimhall, 1988*b*; Bateman, 1992), and isotope ratios (Doe & Delevaux, 1973; Kistler & Peterman, 1973, 1978; DePaolo, 1980, 1981; Masi *et al.*, 1981; Saleeby *et al.*, 1987; Kistler, 1990; Kistler & Ross, 1990; Chen & Tilton, 1991; Kistler & Fleck, 1994; Ducea, 2001; Wenner & Coleman, 2004). Besides lateral variations in magma chemistry, recent geochemical studies of xenoliths (Fig. 2a) and deep crustal exposures suggest pronounced vertical zonation in the geochemistry of the batholith as well (Mukhopadhyay & Manton, 1994; Ducea, 1998, 2001, 2002; Lee *et al.*, 2000; Saleeby *et al.*, 2003; Lackey *et al.*, 2005).

Various studies have interpreted transverse changes in SNB geochemistry as resulting from heterogeneity in the pre-batholith lithosphere and sub-arc mantle. The classic geochemical boundary in the SNB, the $Sr_i = 0{\cdot}706$ line (Figs 1 and 3), delineates the inferred boundary between accreted Phanerozoic rocks in the western Sierra and Proterozoic continental lithosphere in the eastern Sierra (Kistler, 1990). A second boundary recognized inboard of the 0·706 line is the 'PA/NA break' of Kistler (1990). This break runs through the central Sierra and delineates a cryptic pre-batholithic domain boundary between oceanic 'Panthalassan' (Kistler, 1990) lithosphere to the west and North American lithosphere to the east (Fig. 3). The break is based on the location of the 0·706 line, variations of $\delta^{18}O$(WR), and the location of offset pendants or plutons with similar lithology, age, and chemistry (Kistler, 1990, 1993).

Intrusive suites in the Sierra are the 'microcosms' of the batholith. Suites are often defined from field relations (Bateman, 1992), geochemical, and isotopic zonation (Bateman & Chappell, 1979; Kistler *et al.*, 1986; Bateman, 1992), and similar ages or age progressions in member plutons, such as inward decreasing age in zoned plutonic complexes (Chen & Moore, 1982; Coleman *et al.*, 2004). Because trends in geochemistry and age in some suites mimic trends of those same parameters across the SNB, we conducted detailed sampling in several suites to determine how their magmatic systems relate to the batholith as a whole.

SAMPLE SELECTION, PREPARATION, AND ANALYSIS

Zircon was concentrated by standard crushing, density, and magnetic separation techniques. Least magnetic fractions were concentrated with a Frantz separator. Most samples were originally collected for geochronology (Chen & Moore, 1979, 1982; Ratajeski *et al.*, 2001) and thermochronology (House *et al.*, 1997, 1998, 2001; Stockli *et al.*, 2003) studies in the Sierra Nevada and White Mountains. The first author collected samples with '1S' and '3S' prefixes in 2001 and 2003, respectively (see Table 1). Electronic Appendix 1 (available for downloading at http://www.petrology.oxfordjournals.org/) provides details of location, lithological description, and researcher for all samples. Detailed discussion of sampling and mineral separation techniques for the earlier studies is given in the original papers.

Zircon was prepared for $\delta^{18}O$ analysis by sequential acid leaching in HNO_3, HF, and HCl, as described by Lackey *et al.* (2006). HF preferentially dissolves radiation-damaged domains from zircon, which are subject to alteration of $\delta^{18}O$, but does not affect crystalline zircon which preserves pristine $\delta^{18}O$ (King & Valley, 2001; Valley, 2003). Hand-picking under a binocular microscope further purified zircon separates. For each analysis, comprising tens to hundreds of crystals, zircon was powdered using a boron carbide mortar and pestle before laser fluorination.

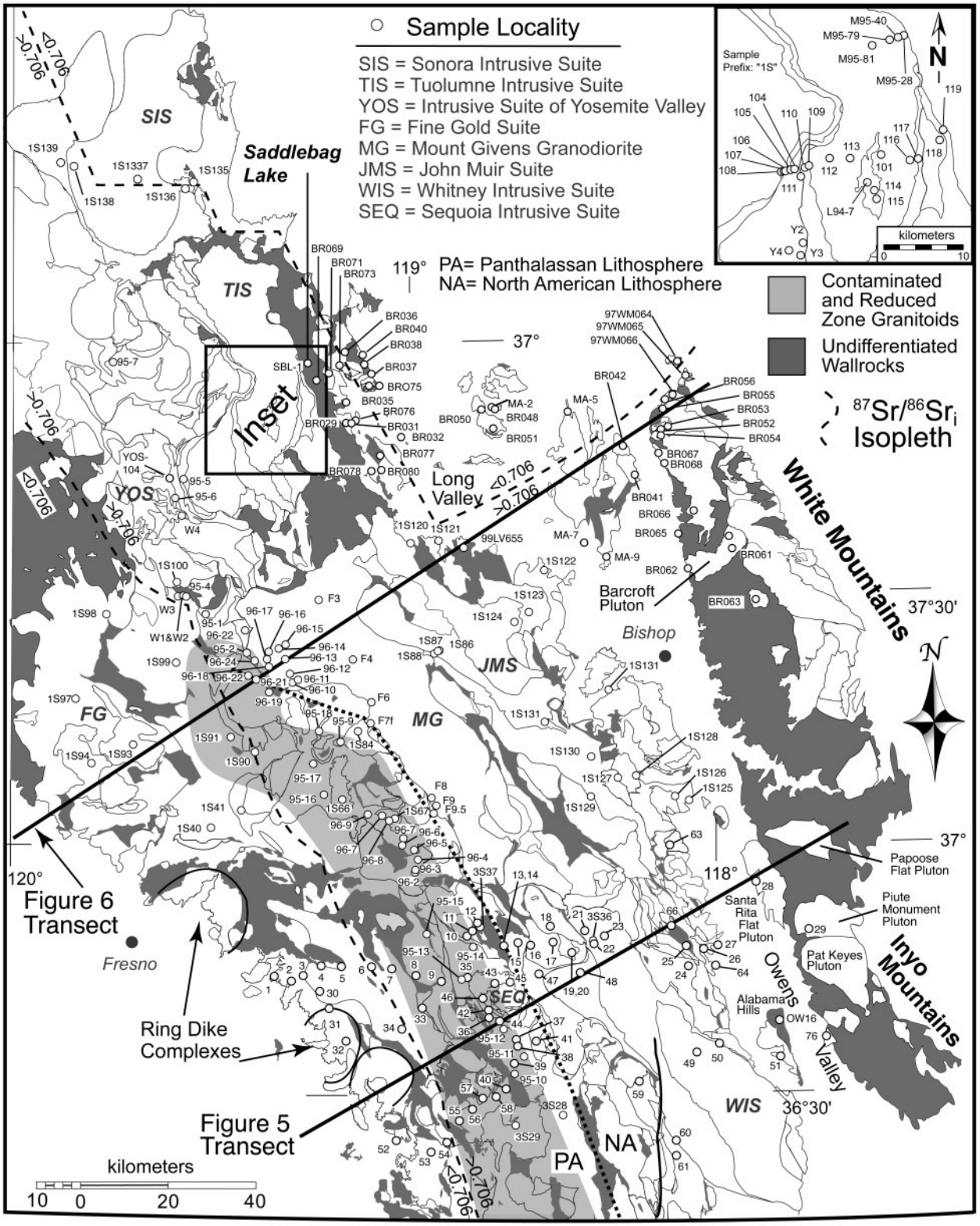

Fig. 3. Geology of the central Sierra Nevada. Sample locations, plutons, the 0·706 line, and the Panthalassan–North American (PA/NA) break of Kistler (1990) are shown, along with the location of the transects of Figs 5 and 6. Details of Sequoia region samples 1–76 have been given by Chen & Moore (1982). Map after Jennings *et al.* (1977), Robinson & Kistler (1986), Kistler (1990), Bateman (1992), Clemens-Knott (1992), Saleeby & Busby (1993), and Moore (2000).

Table 1: Oxygen isotope ratios of zircon, quartz, and whole-rock in the central Sierra Nevada

Sample*	Zircon grain size	Pluton/unit*†	Age* (Ma)	SiO_2 wt %	$\delta^{18}O$ (Zrc)	±1 SD	n‡	$\delta^{18}O$ (Qtz)	±1 SD	n	$\delta^{18}O$ (WR)	Sample*	Zircon grain size	Pluton/unit*†	Age* (Ma)	SiO_2 wt %	$\delta^{18}O$ (Zrc)	±1 SD	n	$\delta^{18}O$ (Qtz)	±1 SD	n	$\delta^{18}O$ (WR)
Western Sierra																							
Kaweah Region																							
W34	<74 µm	unnamed—Three Rivers	98	70·3	7·05	0·01	2	—			8·98	W30	<74 µm	unnamed—Lake Kaweah	112	71·5	6·90	0·16	2	—			9·20
W34	74–149 µm				7·11	0·03	2					W26	<74 µm	unnamed—Sand Creek Rd	115	57·6	6·49	0·01	2	—			7·05
W21	Bulk	unnamed—Pine Flat Rd	100	—	7·04	0·13	2	—			—	W26	74–149 µm				6·49	0·03	2				
W18	<74 µm	unnamed—Pippin Flat	101	—	6·82	0·07	2				8·05	W26	>149 µm				6·43	0·05	2				
W18	74–149 µm				6·83	0·06	2					W29	<74 µm	unnamed—Narañjo	116	—	6·29	0·05	2	—			—
W19	<74 µm	Grd of Hartland	97	61·0	7·51	0·01	2	—			8·70	W29	74–149 µm				6·38	0·04	2				
W19	74–149 µm				7·43	0·02	2					W16	<74 µm	unnamed—Moore Creek Rd	119	58·8	5·73	0·03	2	—			6·76
W32	<74 µm	Tonalite of Pierce Drive	104	66·0	7·11	0·03	2	—			8·78	W16	74–149 µm				5·88	0·03	2				
W32	74–149 µm				7·13	0·03	2					W6	<45 µm	Grt of Grant Grove	126	75·0	7·96	0·04	2	—			10·2
W36	<74 µm	Boyden Cave Pendant	105	—	7·15	0·01	2	—			—	W6	45–74 µm				8·03	0·07	2				
W31	45–74 µm	Tonalite of Pierce Drive	108	57·4	7·08	0·01	2	—			7·94	W6	74–149 µm				8·07	0·00	2				
W22	74–149 µm	unnamed—Squaw Valley	111	—	5·85	0·02	2	—			—	W5	<45 µm	unnamed—Mill Creek	145	72·2	6·20	0·11	2	—			8·06
W22	>149 µm				5·86	0·02	2					W5	45–74 µm				6·09	0·09	2				
W24	74–149 µm	unnamed—Sand Creek Rd	111	63·3	7·30	0·03	2	—			7·56												
W24	>149 µm				7·35	0·06	2																
Fine Gold Intrusive Suite																							
1S94	Bulk	Grd of Knowles	112	72·35	8·08	0·13	2	11·74	0·09	2	10·41	1S99	<74 µm	Bass Lake Tonalite	108	65·95	7·24	0·06	2	10·31	0·12	2	8·46
1S40	<53 µm	Bass Lake Tonalite	112	63·36	7·91	0·01	2	11·04	0·09	2	9·51	1S99	>149 µm				7·18	0·01	2				
1S40	>149 µm				7·81	0·01	2					1S100	< 53 µm	Bass Lake Tonalite	108	62·20	6·71	0·00	2	9·76	0·08	2	8·28

(continued)

Table 1: Continued

Sample*	Zircon grain size	Pluton/unit*†	Age* (Ma)	SiO_2 wt %	$\delta^{18}O$ (Zrc)	±1 SD	n‡	$\delta^{18}O$ (Qtz)	±1 SD	n	$\delta^{18}O$ (WR)	Sample*	Zircon grain size	Pluton/unit*†	Age* (Ma)	SiO_2 wt %	$\delta^{18}O$ (Zrc)	±1 SD	n	$\delta^{18}O$ (Qtz)	±1 SD	n	$\delta^{18}O$ (WR)
1S91	<53 μm	Bass Lake Tonalite	114	67·16	7·30	0·03	2	10·34	0·11	2	8·84	1S100	>149 μm	Bass Lake Tonalite			6·67	0·06	2				
1S91	>149 μm				7·17	0·01	2					W1-H	Bulk	Bass Lake Tonalite	108	—	6·96	0·04	1	—			—
1S97	<53 μm	Bass Lake Tonalite	111	57·85	8·70	0·17	2	12·70	0·16	2	10·76	W2-H	Bulk	Bass Lake Tonalite	108	—	6·35	0·13	2	—			—
1S97	>149 μm				8·44	0·03	2					W3-H	Bulk	Bass Lake Tonalite	108	—	6·90	0·09	2	—			—
1S98	<53 μm	Bass Lake Tonalite	116	63·11	7·79	0·01	2	11·32	0·06	2	9·17	95–4	Bulk	Bass Lake Tonalite	108	—	7·00	0·02	2	—			—
1S98	>149 μm				7·87	0·03	2					95–7	Bulk	Bass Lake Tonalite	115	—	6·27	0·02	2	—			—
Central Sierra																							
Yosemite Intrusive Suite																							
1S103	Bulk	El Capitan Grt	104	73·66	6·46	0·01	2	9·74	0·01	2	9·02	YOS-206	Bulk	Diorite of the Rockslides	102	55·9	6·97	0·00	2	10·42	0·00		7·82
95–6	Bulk	El Capitan Grt	103	—	7·01	0·01	2	—			—	W4	Bulk	Grd of Illilouette Creek	100	—	7·77	0·03	1	—			—
YOS-180	Bulk	El Capitan Grt	104	72·4	5·43	0·08	1	9·40	0·12		8·15	ISP 182	45–62 μm	Grd of Illilouette Creek	99	—	6·66	0·00	2	—			—
YOS-1	Bulk	Taft Grt	103	73·3	6·54	0·08	1	9·14	0·07		8·48	ISP 182	62–80 μm				6·80	0·00	2	—			—
YOS-104	Bulk	North America Wall Diorite	103	55·8	6·68	0·05	2	10·44	0·02		7·75												
Shaver Lake Intrusive Suite, Dinkey Creek Granodiorite																							
95–9	Bulk	Grd of Red Lake	90	—	8·25	0·06	2	—			—	F9·5	Bulk	Dinkey Creek Grd	102	—	7·43	0·04	1	—			—
1S84	Bulk	Grd of Red Lake	90	69·59	7·36	0·01	2	10·89	0·06	2	8·79	95–1	Bulk	Grt of Shuteye Peak	102	—	6·75	0·02	2	—			—
95–18	Bulk	Grt Sheepthief Creek	90	—	7·18	0·06	2	—			—	95–2	Bulk	Grt of Shuteye Peak	102	—	7·58	0·03	2	—			—
1S41	<149 μm	LGrt of Big Sandy Bluffs	93	65·25	7·40	0·00	2	10·59	0·05	2	8·92	96–24	Bulk	Grt of Shuteye Peak	102	—	7·08	0·32	2	—			—
1S41	>149 μm				7·47	0·03	2			2		1S90	<53 μm	Grt of Shuteye Peak	102	71·87	6·53	0·11	2	10·23	0·06	2	9·12
95–16	Bulk	Dinkey Creek Grd	102	—	7·35	0·01	2	—			—	1S90	>149 μm				6·89	0·06					
95–17	Bulk	Dinkey Creek Grd	102	—	7·32	0·09	2	—			—	96–19	Bulk	Grd of Whisky Ridge	103	—	6·73	0·08	2	—			—
96–5	Bulk	Dinkey Creek Grd	102	—	7·44	0·01	2	—			—	96–20	Bulk	Grd of Whisky Ridge	103	—	6·73	0·02	2	—			—
96–6	Bulk	Dinkey Creek Grd	102	—	7·42	0·04	2	—			—	96–21	Bulk	Grd of Whisky Ridge	103	—	6·62	0·12	2	—			—

96-7	Bulk	Dinkey Creek Grd	102	—	7·58	0·04	2	—	—	96-2	Bulk	Grd of McKinley Grove	103	—	7·65	0·11	2	—	—
96-8	Bulk	Dinkey Creek Grd	102	—	7·49	0·03	2	—	—	96-3	Bulk	Grd of McKinley Grove	103	—	7·59	0·1	2	—	—
96-9	Bulk	Dinkey Creek Grd	102	—	7·28	0·01	2	—	—	96-4	Bulk	Grd of McKinley Grove	103	—	7·28	0·13	2	—	—
Mount Givens pluton																			
96-10	Bulk	Mount Givens Grd	90	—	6·64	0·04	1	—	—	96-17	Bulk	Mount Givens Grd	90	—	6·65	0·05	2	—	—
96-11	Bulk	Mount Givens Grd	90	—	6·76	0·04	1	—	—	96-18	Bulk	Mount Givens Grd	90	—	7·07	0·06	2	—	—
96-12	Bulk	Mount Givens Grd	90	—	7·20	0·03	2	—	—	F3	Bulk	Mount Givens Grd	90	—	6·25	0·04	1	—	—
96-13	Bulk	Mount Givens Grd	90	—	6·63	0·02	2	—	—	F4	Bulk	Mount Givens Grd	90	—	6·65	0·04	1	—	—
96-14	Bulk	Mount Givens Grd	90	—	6·49	0·02	2	—	—	F6	Bulk	Mount Givens Grd	90	—	7·36	0·04	2	—	—
96-15	Bulk	Mount Givens Grd	90	—	6·51	0·07	2	—	—	F7f	Bulk	Mount Givens Grd	90	—	7·06	0·04	1	—	—
96-16	Bulk	Mount Givens Grd	90	—	6·68	0·03	2	—	—	F9	Bulk	Mount Givens Grd	90	—	7·03	0·03	1	—	—
Kings Canyon																			
K1	Bulk	Grd of Tehipite Dome	K	—	6·46	0·04	1	—	—	82JB2	60–80 µm	Grd of Tombstone Creek	102	—	7·38	0·04	2	—	—
KC14	<45 µm	North Mountain Stock	89	69·7	5·41	0·04	2			KC18	<45 µm	Grd of Tombstone Creek	99	62·8	7·50	0·03	2	—	8·05
KC14	45–74 µm				5·33	0·05	2			KC18	45–74 µm				7·44	0·02	2		
KC14	74–149 µm				5·28	0·03	2			KC18	74–149 µm				7·41	0·05	2		
KC14-2	45–74 µm	North Mountain Stock	89	—	5·47	0·01	2	—	—	82CNK107A	45–80 µm	Boyden Cave Pendant	102	—	5·55	0·01	2	—	—
KC14-2	74–149 µm				5·54	0·00	2			82CNK108A	45–80 µm	Grt of Grand Dike	103	—	7·41	0·00	2	—	—
K2	Bulk	Grd of North Dome	90	—	6·56	0·06	2	—	—	82JB1	45–62 µm	Boyden Cave Pendant	105	—	7·74	0·05	2	—	—
KC22	—	Grd of North Dome	90	—	—			—	7·99	82JB 004	45–80 µm	Boyden Cave Pendant	106	—	7·32	0·01	2	—	—
SQ67	45–74 µm	Grd of Mitchell Peak	91	61·0	5·85	0·02	2	—	7·21	82JB 004	80–120 µm				7·39	0·02	2		
SQ67	74–149 µm				5·81	0·03	2			KC16	74–149 µm	Grd of Lightning Creek	108	62·5	7·10	0·06	2	—	8·34
KC2	45–74 µm	Grd of Lookout Peak	97	—	6·10	0·01	2	—	—	KC6	45–74 µm	Qtz Drt of Yucca Point	110	62·7	7·59	0·01	2	—	9·49
KC2	>74 µm				6·14	0·02	2			KC6	>74 µm				7·67	0·02	2		
K4	Bulk	Grd of Lookout Peak	97	—	6·50	0·03	1	—	—	KC11	Bulk	Qtz Drt of Yucca Point	110	—	7·64	0·06	2	—	—

(continued)

Table 1: Continued

Sample*	Zircon grain size	Pluton/unit*†	Age* (Ma)	SiO_2 wt %	$\delta^{18}O$ (Zrc)	±1 SD	*n*‡	$\delta^{18}O$ (Qtz)	±1 SD	*n*	$\delta^{18}O$ (WR)
KC15	<45 μm	Grd of Lookout Peak	97	69·1	6·00	0·01	2	—			7·71
KC15	45–74 μm				5·99	0·01	2				
KC15	74–149 μm				6·05	0·01	2				
KC5	45–74 μm	Grd of Tombstone Creek	99	—	7·30	0·06	2	—			—
KC5	>74 μm				7·38	0·02	2				
Sequoia National Park											
3S28	Bulk	Grd of Castle Creek	97	65·00	6·28	0·03	2	9·76	0·01		7·92
3S29	Bulk	Grt of Case Mt.	100	68·63	7·07	0·02	2	10·09	0·05		8·70
W2		Grt of Grant Grove	106	—	—			—			10·76
SQ12	42	Grt of Big Meadows	98	67·5	6·73	0·03	2	—			8·67
SQ46	45–74 μm	Grt of Big Meadows	98	66·0	6·62	0·03	2	—			8·57
SQ46	>74 μm				6·62	0·01	2				
SQ48	Bulk	Grt of Big Meadows	98	69·3	6·69	0·01	2	—			8·39
SQ13	45–74 μm	Giant Forest Grd	97	69·1	6·53	0·03	2	—			8·68
SQ13	>74 μm				6·80	0·01	2				
SQ22	45–74 μm	Giant Forest Grd	97	—	6·72	0·02	2	—			—
SQ22	74–149 μm				6·78	0·05	2				
SQ57	<45 μm	Giant Forest Grd	100	60·7	7·04	0·01	2	—			8·07
SQ57	45–74 μm				7·01	0·01	2				
SQ7	Bulk	Giant Forest Grd	102	—	7·05	0·12	2	—			—
SQ75	Bulk	Giant Forest Grd	100	70·2	7·12	0·05	2	—			8·30
SQ9	45–74 μm	Giant Forest Grd	100	—	7·18	0·03	2	—			—
95–10	Bulk	Giant Forest Grd	102	—	6·90	0·03	2	—			—

Sample*	Zircon grain size	Pluton/unit*†	Age* (Ma)	SiO_2 wt %	$\delta^{18}O$ (Zrc)	±1 SD	*n*	$\delta^{18}O$ (Qtz)	±1 SD	*n*	$\delta^{18}O$ (WR)
F11	Bulk	Qtz Drt of Yucca Point	110	—	7·70	0·03	1	—			—
KC42	<74 μm			—	7·27	0·02	2	—			—
KC42	74–149 μm				7·27	0·01	2				
KC42	>149 μm				7·41	0·05	2				
3S37	Bulk	Grd of Brush Canyon	86	73·11	8·39	0·08	2	11·96	0·07		10·95
95–11	Bulk	Giant Forest Grd	102	—	6·83	0·02	2	—			—
95–12	Bulk	Giant Forest Grd	102	—	6·76	0·03	2	—			—
95–13	Bulk	Giant Forest Grd	102	—	6·64	0·03	2	—			—
95–14	Bulk	Giant Forest Grd	102	—	6·59	0·01	2	—			—
SQ15	<45 μm	Grd of Milk Ranch Peak	99	70·2	7·48	0·02	2	—			9·76
SQ15	45–74 μm				7·48	0·02	2				
SQ5	Bulk	Grd of Milk Ranch Peak	97	—	7·42	0·02	1	—			—
SQ3	45–74 μm	Grt of Frys Point	99	—	7·61	0·02	2	—			—
SQ61	46 μm	Grt of Weaver Lake	100	77·9	6·75	0·04	1	—			9·32
89KK2	62–80 μm	Redwood Mt. Pendant	105	—	7·21	0·03	2	—			—
89KK4	62–80 μm	Redwood Mt. Pendant	105	—	7·34	0·04	2	—			—
SQ8	<45 μm	Grt of Lodgepole Campgrd.	111	68·7	7·63	0·02	2	—			9·34
SQ8	45–74 μm				7·60	0·02	2				
SQ8	74–149 μm				7·67	0·05	2				
89KK5	80–100 μm	unnamed Grd	115	—	5·70	0·11	2	—			—
89KK1a	45–62 μm	Grd of Yucca Mt.	162	—	5·81	0·01	2	—			—

Eastern Sierra																							
Tuolumne Intrusive Suite																							
1S106	Bulk	Glen Aulin Tonalite	93·3	62·67	6·39	0·00	2	9·45	0·12	2	7·74	1S110	Bulk	Half Dome Grd (porph.)	88·8	69·52	6·30	0·01	2	9·35	0·01	2	8·39
1S107	Bulk	Glen Aulin Tonalite	93·3	58·61	6·29	0·01	2	9·30	0·05	2	7·05	1S116	Bulk	Half Dome Grd (porph.)	88·8	67·51	6·38	0·03	2	9·77	0·12	2	8·21
1S108	Bulk	Glen Aulin Tonalite	93·3	57·64	6·35	0·01	2	9·41	0·00	2	7·44	1S101	Bulk	Cathedral Peak Grd	88·1	71·46	6·49	0·07	2	9·34	0·05	2	8·51
1S119	Bulk	Kuna Crest Grd	93·3	66·48	6·20	0·01	2	9·96	0·02	2	7·75	1S112	Bulk	Cathedral Peak Grd	88·1	67·55	6·51	0·08	2	9·58	0·03	2	8·22
95-5	Bulk	Kuna Crest Grd	93·3	—	6·23	0·02	2	—			—	1S113	Bulk	Cathedral Peak Grd	88·1	69·54	6·43	0·05	2	9·52	0·01	2	8·35
1S111	Bulk	Half Dome Grd	91·9	68·19	6·17	0·06	2	9·52	0·13	2	8·11	1S117	Bulk	Cathedral Peak Grd	88·1	66·95	6·31	0·11	2	9·38	0·14	2	8·16
1S118	Bulk	Half Dome Grd	91·9	68·44	6·30	0·04	2	9·74	0·04	2	8·02	M95-28	Bulk	Cathedral Peak Grd	88·1	69·1	6·34	0·05	2	9·79	0·12		8·31
1S104	Bulk	Half Dome Grd	91·9	71·06	6·27	0·07	2	9·03	0·10	2	8·08	M95-40	Bulk	Cathedral Peak Grd	88·1	—	6·39	0·03	2	9·65	0·05		7·77
1S105	Bulk	Half Dome Grd	91·9	68·72	6·13	0·06	2	9·01	0·11	2	8·11	M95-79	Bulk	Cathedral Peak Grd	88·1	—	6·30	0·15	2	9·61	0·08		8·26
Y2	Bulk	Half Dome Grd	91·9	—	6·56	0·06	1	—			—	M95-81	Bulk	Cathedral Peak Grd	88·1	—	6·31	0·06	2	9·75	0·05		8·94
Y3	Bulk	Half Dome Grd	91·9	—	6·41	0·06	1	—			—	1S114	Bulk	Johnson Grt Porphyry	85·4	70·96	6·21	0·03	2	9·90	0·06	2	8·79
Y4	Bulk	Half Dome Grd	91·9	—	6·45	0·06	1	—			—	1S115	Bulk	Johnson Grt Porphyry	85·4	76·13	6·51	0·06	1	9·89	0·02	2	9·13
1S109	Bulk	Half Dome Grd (porph.)	88·8	69·18	6·51	0·08	2	9·63	0·00	2	8·51	L94-7	Bulk	Johnson Grt Porphyry	85·4	75·6	6·96	0·09	1	9·63	0·35		9·05
Other Sierra Crest plutons																							
1S127	Bulk	Inconsolable Grd	95	58·45	6·02	0·04	2	9·40	0·04	2	7·16	1S120	Bulk	Mono Creek Grt	87	65·34	6·17	0·03	2	9·72	0·04	2	8·51
1S129	Bulk	Lamark Grd (porph.)	94	65·42	5·65	0·00	2	8·82	0·07	2	5·29	1S124	Bulk	Mono Creek Grt	87	68·19	6·11	0·01	2	9·52	0·04	2	8·03
1S88	Bulk	Lamark Grd	92	62·31	5·84	0·06	2	9·36	0·10	2	7·37	68M15	Bulk	Grd of Sugarloaf	88	62·0	5·90	0·02	2	—			7·37
1S130	Bulk	Lamark Grd	92	63·93	5·84	0·01	2	9·20	0·11	2	7·83	KC13	—	Paradise Grd	85	—	—			—			7·22
1S86	Bulk	Lake Edison Grd (coarse)	90·9	67·42	6·14	0·05	2	9·46	0·01	2	7·94	KC20	—	Paradise Grd	85	—	—			—			7·91
1S87	Bulk	Lake Edison Grd (fine)	90·9	68·72	5·52	0·01	2	8·85	0·05	2	7·17	3S36	Bulk	Paradise Grd	85	67·36	5·70	0·03	2	9·34	0·08		7·50
1S131	Bulk	Lake Edison Grd	90·9	71·00	5·78	0·00	2	8·81	0·02	2	7·90	A95-10	Bulk	Whitney Grd	84	69·7	5·89	0·02	2	8·97	0·15		8·04
LEG 91-536	80–100 µm	Lake Edison Grd	90·9	—	5·99	0·09	3					WHIT	<45 µm	Whitney Grd	84	—	5·67	0·01	3	—			—
1S121	Bulk	Round Valley Peak Grd	88·8	67·79	6·19	0·02	2	9·16	0·04	2	8·38	1S135	Bulk	Grd of Kinney Lake	91	67·53	6·17	0·02	2	9·64	0·09	2	8·25
1S123	Bulk	Round Valley Peak Grd	88·8	67·83	6·32	0·02	2	9·60	0·04	2	7·99	1S139	Bulk	Grd of Kinney Lake	91	67·14	6·44	0·02	2	9·69	0·06	2	8·27
99LV655	<53 µm	Round Valley Peak Grd	88·8	62·6	6·43	0·02	2	9·88	0·21	9	7·76	1S136	Bulk	Grd of Topaz Lake	86	69·17	6·52	0·00	2	9·65	0·04	2	8·12
99LV655	74–105 µm				6·44	0·03	2					1S137	Bulk	Grd of Topaz Lake	86	66·17	6·68	0·01	2	9·97	0·01	2	8·41
99LV655	>149 µm				6·51	0·01	2					1S138	Bulk	Grd of Topaz Lake	86	67·32	6·50	0·02	2	9·62	0·00	2	8·34

(continued)

Table 1: Continued

Sample*	Zircon grain size	Pluton/unit*†	Age* (Ma)	SiO_2 wt %	$\delta^{18}O$ (Zrc)	±1 SD	n‡	$\delta^{18}O$ (Qtz)	±1 SD	n	$\delta^{18}O$ (WR)	Sample*	Zircon grain size	Pluton/unit*†	Age* (Ma)	SiO_2 wt %	$\delta^{18}O$ (Zrc)	±1 SD	n	$\delta^{18}O$ (Qtz)	±1 SD	n	$\delta^{18}O$ (WR)
Miscellaneous Cretaceous: eastern Sierra, Long Valley, Owens Valley																							
1S133	Bulk	Grd of Billy Lake	99	68·20	5·89	0·04	2	9·43	0·01	2	7·34	95BR071	Bulk	LGrt of Ellery Lake	96	—	6·59	0·12	2	—			—
1S134	Bulk	Grd of Rush Creek	99	62·07	5·78	0·02	2	9·89	0·01	2	7·09	95BR032	<53 μm	Qtz Mzd of Aeolian Buttes	96	—	6·07	0·07	1	—			—
95BR076	Bulk	Qtz Mzd of Aeolian Buttes	96	—	4·21	0·02	2	—			—	95BR032	>105 μm				5·97	0·07	1				
95BR035	Bulk	Grt of June Lake	93	—	5·98	0·00	2	—			—	L5P334A	45–80 μm	Grd of Dragon pluton	102	61·1	5·07	0·02	2	—			—
95BR073	Bulk	Grt of June Lake	93	—	5·55	0·03	2	—			—	L5P334A	80–120 μm				4·79	0·02	2				
95BR077	Bulk	Grt of June Lake	93	—	6·07	0·04	2	—			—	OW34	74–149 μm	Grd of Dragon pluton	103	—	5·33	0·03	2	—			—
95BR075	<74 μm	Grt of June Lake	93	—	6·01	0·00	2	—			—	OW4	<45 μm	Grt of Bullfrog pluton	103	—	5·07	0·05	2	—			6·66
95BR075	>149 μm				6·15	0·01	2					OW4	45–74 μm				5·15	0·09	2				
6-124	Bulk	Grt of Mt Kaweah	95	—	4·65	0·11	2	—			—	OW4	74–149 μm				5·21	0·01	2				
95BR037	Bulk	Grt of Mono Lake	96	—	6·75	0·07	1	—			—	L5P333A	45–80 μm	Grt of Arrowhead Lake	105	75·0	4·97	0·07	2	—			—
95BR038	Bulk	Grt of Mono Lake	96	—	6·69	0·02	2	—			—	L4P236A	45–80 μm	Grt of Sardine Pluton	105	71·9	5·40	0·01	2	—			—
95BR040	Bulk	Grt of Mono Lake	96	—	6·70	0·03	2	—			—	OW39	Bulk	Grt of Alabama Hills	85	—	6·41	0·04	2	—			—
95BR069	Bulk	Grd of Tioga Lake	96	—	5·98	0·00	2	—			—	OW7	Bulk	Grt of Independence Pluton	112	74·8	4·61	0·15	2	—			6·60
Jurassic and Triassic: eastern Sierra, Long Valley, Benton Range, Owens Valley																							
MA7	Bulk	Independence Dike	148	70·1	6·90	0·02	2	—			9·57	L4P124A	62–100 μm	Oak Creek Pendant	167	72·1	6·33	0·02	2	—			—
E-27-3	<74 μm	Independence Dike	148	—	5·45	0·07	2	—			9·41	95BR036	<74 μm	Grd of Mono Dome	168	—	7·01	0·00	2	—			—
E-27-3	74–149 μm				5·43	0·1	2					95BR036	>149 μm				7·13	0·05	2				
E-27-8	<74 μm	Independence Dike	148	—	5·48	0·01	2	—				1S132	Bulk	Tungsten Hills Grt	200	71·79	5·48	0·01	2	8·39	0·03	2	7·59
E-27-8	74–149 μm				5·82	0·07	2					OW2	45–74 μm	Tungsten Hills Grt	210	74·4	7·45	0·04	2	—			9·23
OW16	—	Independence Dike	148	—	—			—			−0·52	MA5	<74 μm	Tungsten Hills Grt	201	—	7·23	0·06	2	—			9·32
OW17	—	Independence Dike	148	—	—			—			7·42	MA5	74–149 μm				7·40	0·06	2				
8-38a	Bulk	Qtz Monz of Red Mt. Creek	153	—	7·37	0·04	2	—			—	95BR078	Bulk	Grt of Lee Vining Canyon	210	—	6·24	0·06	2	—			—
8-54	Bulk	Grd of White Fork Pluton	156	71·4	6·29	0·04	2	—			4·86	95BR080	Bulk	Grt of Lee Vining Canyon	210	—	6·67	0·05	2	—			—
77-7	Bulk	Grd of Window Cliffs	159	—	5·60	0·05	2	—			—	95BR029	Bulk	Grt of Lee Vining Canyon	210	—	6·20	0·06	2	—			—

7-19	Bulk	Grd of Window Cliffs	160	—	5·51	0·01	2	—			—	95BR031	<74 μm	Grt of Lee Vining Canyon	210	—	6·06	0·01	2	—			—
95BR042	Bulk	LGrt of Casa Diablo Mt.	161	—	6·83	0·04	2	—			—	95BR031	>149 μm				6·15	0·07	1				
MA9	>74 μm	LGrt of Casa Diablo Mt.	161	66·3	7·2	0·05	2	—			—	95BR048	Bulk	Wheeler Crest Grd	214	—	7·96	0·09	2	—			—
MA9	74–149 μm				7·35	0·03	2					95BR050	Bulk	Wheeler Crest Grd	214	—	6·81	0·06	2	—			—
1S125	Bulk	Grd of McMurray Meadows	164	64·58	6·75	0·05	2	9·88	0·06	2	8·44	95BR051	Bulk	Wheeler Crest Grd	214	—	7·44	0·09	2	—			—
1S126	Bulk	Tinemaha Grd	164	62·81	6·82	0·05	2	9·60	0·09	2	8·11	95BR041	Bulk	Wheeler Crest Grd	214	—	7·06	0·04	2	—			—
OW6	—	Tinemahah Grd (Woods L.)	165	—	—			—			7·84	MA2	<74 μm	Wheeler Crest Grd	217	63·4	6·63	0·01	2	—			8·1
L4P235A	45–80 μm	Oak Creek Pendant	164	—	6·41	0·02	2	—			—	1S122	Bulk	Wheeler Crest Grd	214	72·2	7·01	0·09	2	9·88	0·06	2	8·98
L4P054A	62–100 μm	Oak Creek Pendant	165	71·5	6·34	0·04	2	—			—	SBL-1	Bulk	Saddlebag Lake Rhyolite	222	—	6·22	0·02	2	12·66	0·07	2	11·68
White and Inyo Mountains																							
95BR052	<105 μm	Grt of Boundary Peak	74	—	6·86	0·03	2	—			—	95BR065	Bulk	unnamed metavolcanic	147	—	5·49	0·07	1	—			—
95BR052	>105 μm				6·72	0·01	2					95BR061	Bulk	Qtz Monz of Mt. Barcroft	165	—	7·56	0·02	2	—			—
95BR053	Bulk	Grt of Boundary Peak	74	—	6·54	0·07	2	—			—	95BR062	Bulk	Qtz Monz of Mt. Barcroft	165	—	7·61	0·01	2	—			—
95BR054	Bulk	Grt of Pellisier Flats	90	—	7·48	0·11	2	—			—	95BR064	Bulk	Qtz Monz of Mt. Barcroft	165	—	7·63	0·06	2	—			—
95BR055	Bulk	Grt of Pellisier Flats	90	—	7·03	0·03	2	—			—	95BR063	Bulk	Grt of Sagehen Flat	175	—	7·26	0·03	2	—			—
95BR056	Bulk	Grt of Pellisier Flats	90	—	6·57	0·02	2	—			—	E-27-9	<74 μm	Grt of Paiute Monument	152	—	6·68	0·01	2	—			—
95BR066	Bulk	Grt of Pellisier Flats	90	—	6·38	0·02	2	—			—	OW35	Bulk				6·39	0·09	2				
95BR067	<53 μm	Grt of Pellisier Flats	90	—	6·55	0·04	2	—			—	OW36	Bulk	Poisen Canyon		—	5·3	0·06	2	—			8·99
95BR067	<105 μm				6·56	0·01	2					OW19	<45 μm	Santa Rita Flat	163	63·0	6·84	0·02	2	—			8·43
95BR068	Bulk	Grt of Pellisier Flats	90	—	6·78	0·05	2	—			—		45–74 μm				6·81	0·02	2				
97WM064	<53 μm	Grt of Pellisier Flats	90	—	6·82	0·03	2	—			—		74–149 μm				6·76	0·01	2				
97WM064	>149 μm				6·83	0·04	2					F1-57	Bulk	Mzt of Long John Pluton	175	—	6·44	0·06	2	—			—
97WM065	Bulk	Grt of Pellisier Flats	90	—	6·92	0·06	2	—			—	02–26	74–149 μm	Mzt of Darwin Stock	175	—	6·99	0·06	2	—			—
97WM066	Bulk	Grt of Pellisier Flats	90	—	6·95	0·02	2	—			—												

*Detailed sample locations, descriptions, and geochronology references are given in Electronic Appendix 1. Analytical methods are detailed in the text. Oxygen isotope ratios are ‰ relative to Vienna Standard Mean Ocean Water (VSMOW).
†Abbreviations: Grd, granodiorite; Grt, granite; Mzt, monzonite; Drt, diorite; Mzd, monzodiorite; LGrt, leucogranite; Qtz Monz, quartz monzonite; L., lake; Mt., mount; Rd, Road; porph., porphyritic.
‡*n* denotes number of analyses.
Samples with prefixes ISP, 89KK, L4P, L5P, 82, WHIT and LEG are from Lackey *et al*. (2005).

Powdering creates uniform size and increases fluorination efficiency.

Mineral separates and whole-rock powders were analyzed in the University of Wisconsin Stable Isotope Laboratory by laser fluorination. Isotope ratios were measured on a dual inlet gas source Finnigan MAT 251 mass spectrometer. Whole-rock powders (2–2·5 mg) were analyzed with an airlock sample chamber (Spicuzza *et al.*, 1998). Oxygen was liberated from silicates with BrF_5 using a 30W CO_2 laser ($\lambda = 10{\cdot}6\ \mu m$), then purified cryogenically, passed through hot Hg to remove any residual F_2, and finally converted to CO_2 with a hot carbon rod (Valley *et al.*, 1995). All analyses were standardized daily based on four or more analyses of UWG-2, Gore Mountain garnet standard, and sample $\delta^{18}O$ values were corrected to the long-term accepted value of 5·80‰ for UWG-2. The average raw $\delta^{18}O$ of UWG-2 for 40 days of analyses ($n = 217$) in this study is 5·71 ±0·13‰ [1SD; standard error ($1\sigma = 1SD/(n^2)$ is ±0·009‰]. Average day-to-day precision of UWG-2 is ± 0·06‰; daily corrections average 0·08‰. Average $\delta^{18}O$ of NBS-28 run on 7 days was 9·45 ± 0·13‰ after correction, $n = 20$, and Δ(NBS-28–UWG-2) averaged 3·65 ± 0·12‰, in excellent agreement with the UW laboratory long-term Δ(NBS-28–UWG-2) of 3·70 ± 0·06‰ (1SD) (Valley *et al.*, 1995). During 9 days of whole-rock analyses using the airlock chamber, UWG-2 averaged 5·67 ± 0·11‰ ($n = 41$); replicate analyses of whole-rock powders averaged ±0·11‰. Replicate analyses give uncertainties of less than ±0·04% for zircon and ±0·09% for quartz.

Major elements and selected trace elements (Rb, Sr, Y, Nb, Zr) were determined for 96 samples by X-ray fluorescence at XRAL Laboratories, Canada. These data and discussion of analytical techniques are provided in Electronic Appendix 2.

Comparison of the $\delta^{18}O$ values of mineral pairs with equilibrium fractionation factors is used in several sections of the paper to test if minerals have exchanged oxygen, and the degree to which they approach isotopic equilibrium. Isotopic fractionation factors are expressed as

$$\Delta_{i-j} = \delta^{18}O(\text{mineral-}i) - \delta^{18}O(\text{mineral-}j) \approx 1000 \ln \alpha(i-j).$$

Equilibrium fractionation factors are calculated for a particular temperature using the expression

$$1000 \ln \alpha(\text{mineral-}i - \text{mineral-}j) \approx \frac{A_{i-j} \times 10^6}{T^2}$$

where T is temperature (K) and A is an experimentally or empirically determined coefficient. The following A factors are used for oxygen isotopes: quartz–zircon = 2·64 (Valley *et al.*, 2003); quartz–plagioclase = 1·20 (Clayton *et al.*, 1989); quartz–K-feldspar = 1·00 (Clayton *et al.*, 1989); quartz–biotite = 2·16 (Chacko *et al.*, 2001); quartz–hornblende = 3·01 by combining the fractionation factors quartz–almandine (Valley *et al.*, 2003) and garnet–hornblende (Kohn & Valley, 1998).

RESULTS

Oxygen isotope ratios

Zircon

Zircon $\delta^{18}O$ in the study area ranges from 4·2 to 9·2‰ (Table 1). Variation of $\delta^{18}O$ is presented both as a color-coded map of the central Sierra (Fig. 4), and as two east–west transects (Figs 5 and 6) that divide the data approximately between the Fresno (Fig. 5; 36–37°N) and Mariposa (Fig. 6; 37–38°) 1/250 000 sheets (Fig. 1).

Values span most of the terrestrial range for $\delta^{18}O$ of igneous zircon in plutonic rocks (Valley *et al.*, 2005); 94% are above the mantle value for zircon (5·3 ± 0·3‰, 1SD; Valley *et al.*, 1998), and the rest are in or slightly below the mantle range. Comparison of $\delta^{18}O$ variation between different grain-size fractions of zircon (see Table 1) reveals no consistent pattern of size versus $\delta^{18}O$ within samples (Lackey, 2005). Intra-pluton $\delta^{18}O$ variations typically are small, <0·3‰ (Table 1), and comparable with the range of $\delta^{18}O$(Zrc) from volcanic systems with relatively simple zircon crystallization histories. For example, the Bishop Tuff varies by only 0·21‰ between early and late erupted units (Bindeman & Valley, 2002). The Mount Givens, Bass Lake, and Giant Forest Plutons are zoned in $\delta^{18}O$ (Figs 3 and 4).

Whole-rocks

Measured $\delta^{18}O$(WR) across the central Sierra varies from 6 to 11·7‰, with one value as low as −0·5‰ (Table 1). The range of $\delta^{18}O$(WR) values is larger than previously reported in the central Sierra (Masi *et al.*, 1981; Kistler, 1990). Overall, this study adds considerably to the coverage of $\delta^{18}O$(WR) in the Fresno sheet (Fig. 5b), and doubles the data for the Mariposa sheet (Fig. 6b), which increases the known range of $\delta^{18}O$(WR).

Quartz

Values of $\delta^{18}O$(Qtz) were analyzed from rocks throughout the central Sierra. The range of $\delta^{18}O$(Qtz) is 8·8–12·0‰. Distribution of oxygen isotopes between coexisting quartz and zircon yields apparent temperatures of 575–650°C, which are significantly lower than are expected for magmatic crystallization (850–650°, Fig. 7). Similar $\Delta^{18}O$(Qtz–Zrc) disequilibrium is recognized in the Idaho batholith (King & Valley, 2001) and is explained by closed-system resetting of $\delta^{18}O$(Qtz) during sub-solidus cooling, owing to relatively fast oxygen diffusion in quartz (Farver & Yund, 1991; Sharp *et al.*, 1991), which yields a lower closure temperature (Dodson, 1973) for oxygen exchange in quartz than in zircon.

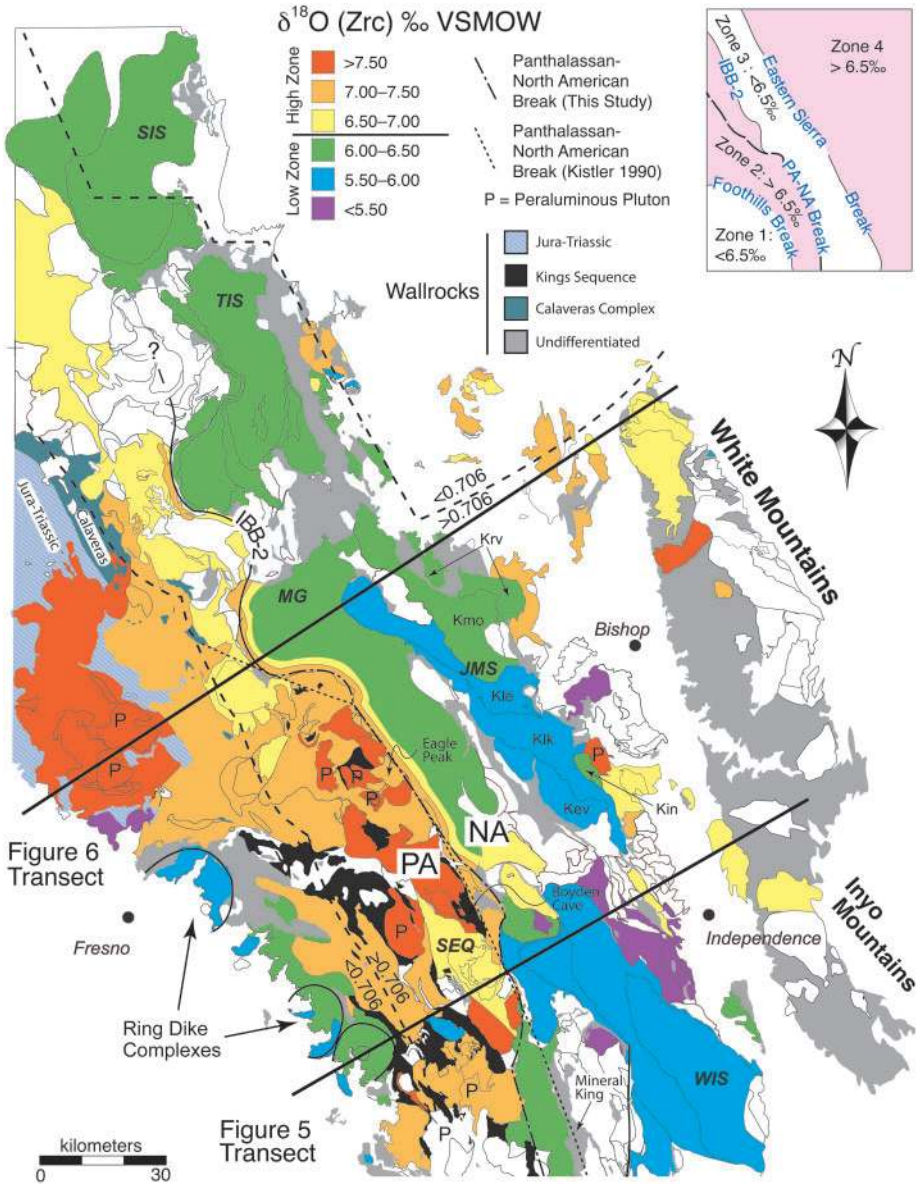

Fig. 4. $\delta^{18}O$(Zrc) in the central Sierra Nevada. Four prominent high- and low-$\delta^{18}O$ belts (Zones 1–4) are recognized (see inset). Zoning of $\delta^{18}O$ in the Mount Givens pluton shown as $\delta^{18}O$ zones along its west side. The significance of the Eagle Peak pluton, Boyden Cave, and Mineral King pendants is discussed in the text. P, peraluminous pluton; IBB-2, Intrabatholithic Break; 2. John Muir Suite includes: Kin, Inconsolable Granodiorite; Klk, Lamark Granodiorite; Kle, Lake Edison Granodiorite; Krv, Round Valley Peak Granodiorite; Kmo, Mono Creek Granite.

Oxygen isotope mapping of the Central Sierra Nevada

High sampling density, homogeneity of $\delta^{18}O$ in most plutons, and thorough mapping allow us to present the results as a detailed isotopic map of the central SNB (Fig. 4). This representation both shows regional $\delta^{18}O$ variations and resolves isotopic zoning of intrusive suites with detail beyond simple contouring of $\delta^{18}O$. Except where $\delta^{18}O$ varies by >0·5‰, values were averaged for plutons having multiple samples. An overarching pattern emerges with four north–south running belts of rocks having $\delta^{18}O$(Zrc) that is greater or less than 6·5‰ (inset, Fig. 4). Nonetheless, there is substantial heterogeneity within the belts, including on-strike changes of $\delta^{18}O$ (see 'Regional $\delta^{18}O$ belts' below).

DISCUSSION

Relating $\delta^{18}O$(Zrc) to $\delta^{18}O$(WR)

Correlation with SiO_2

To use zircon as a benchmark for evaluating the degree of contamination or sub-solidus alteration, the fractionation

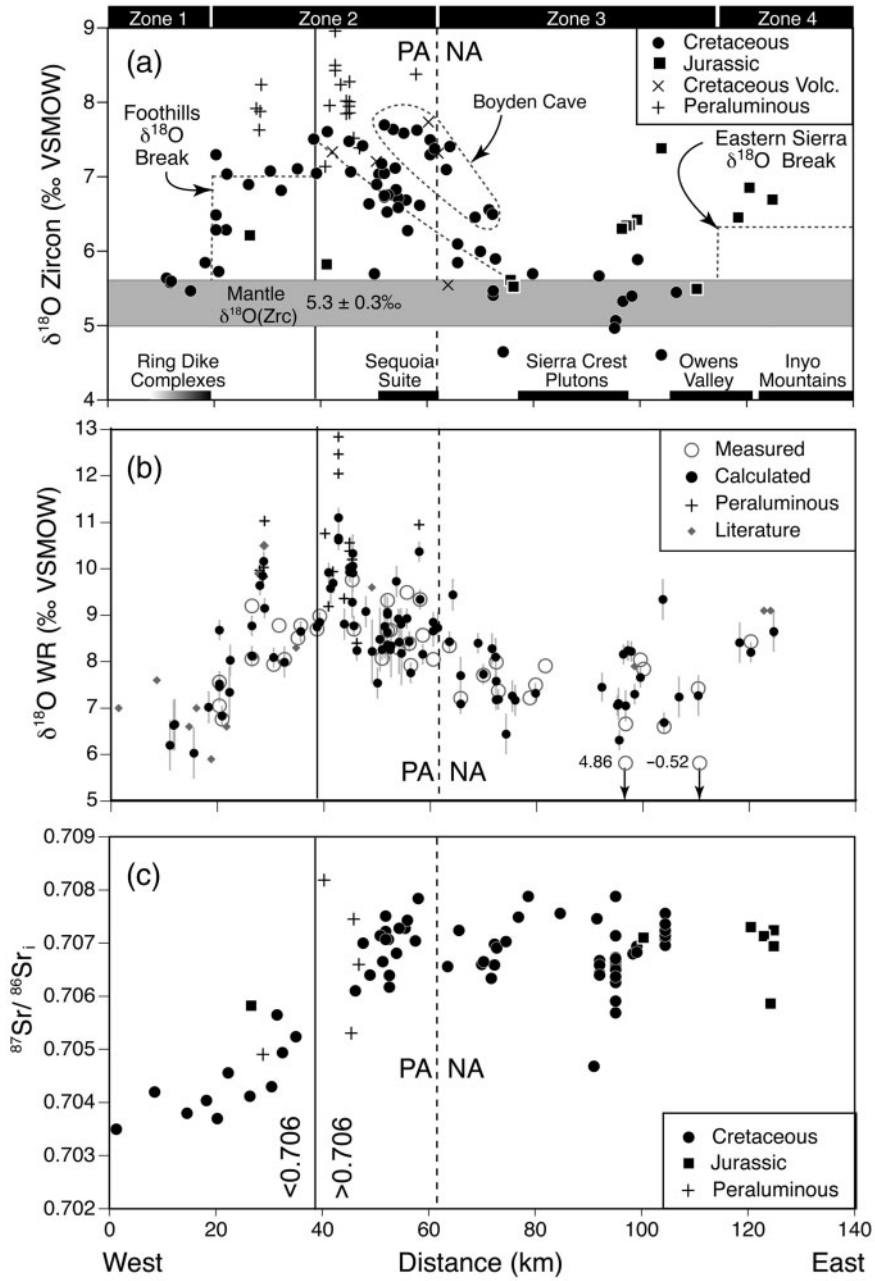

Fig. 5. Fresno sheet transect showing (a) $\delta^{18}O$(Zrc). (b) Measured and calculated $\delta^{18}O$(WR). (c) Initial $^{87}Sr/^{86}Sr$. (Note location of 0·706 line, Foothills Break, and PA/NA break.) Error bars on calculated $\delta^{18}O$ are 1SD and reflect greater uncertainty of values of samples for which SiO_2 was estimated. Published data are from sources listed in Fig. 2 and Chen & Tilton (1991), Sisson *et al.* (1996), Coleman & Glazner (1997), Wenner & Coleman (2004), and Lackey *et al.* (2005, 2006).

of $\delta^{18}O$(Zrc) and $\delta^{18}O$(WR) at magmatic temperatures must be calibrated. Overall, measured $\delta^{18}O$(WR) correlates with $\delta^{18}O$(Zrc), but $\delta^{18}O$(WR) is more variable and 0·5–3·0‰ higher (Fig. 8a; Table 1). Values of $\delta^{18}O$(WR) positively correlate with SiO_2 content and $\delta^{18}O$(Zrc) has a slight positive correlation. The high variance in Fig. 8a reflects differences of magmatic $\delta^{18}O$ throughout the central Sierra Nevada.

Values of $\delta^{18}O$(Zrc) are independent of wt % SiO_2 in the Tuolumne Intrusive Suite, with one outlier, whereas $\delta^{18}O$(WR) is positively correlated and varies by over 2·0‰ from 57 to 76 wt % SiO_2 (Fig. 8a). Mafic magmas undergoing closed-system differentiation typically see $\delta^{18}O$(WR) increase by 0·5‰ for each 10% increase in SiO_2 (Taylor & Sheppard, 1986); however, results from the Tuolumne suite indicate that $\delta^{18}O$(WR) in calc-alkaline

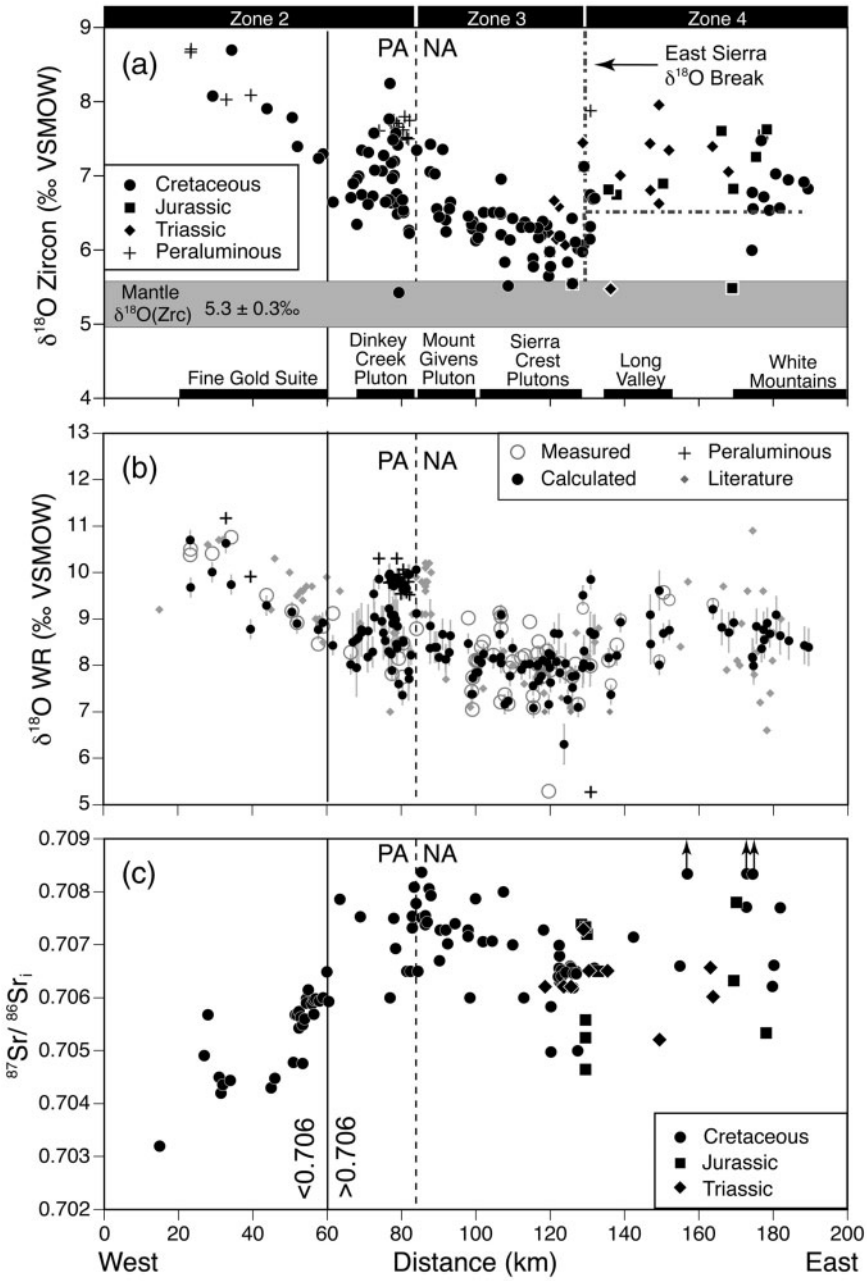

Fig. 6. Mariposa sheet transect showing (a) $\delta^{18}O$(Zrc), (b) measured and calculated $\delta^{18}O$(WR), and (c) initial $^{87}Sr/^{86}Sr$. Major features and boundaries are as in Fig. 3. Published data are from sources listed in Fig. 2 and Hill *et al.* (1988), Bateman *et al.* (1991), Coleman *et al.* (1992), Coleman & Glazner (1997), Ratajeski *et al.* (2001), Ernst & Rumble (2003), Ernst *et al.* (2003), Wenner & Coleman (2004), and Lackey *et al.* (2005, 2006).

systems increases by ~1·0‰ for each 10% increase of SiO_2. In general, increasing SiO_2 in calc-alkaline igneous rocks correlates with increasing modal abundance of high-$\delta^{18}O$ minerals such as quartz and feldspar, and with decreasing amounts of lower $\delta^{18}O$ minerals such as amphibole, biotite, and magnetite. The Tuolumne suite exemplifies how differentiation creates variability of $\delta^{18}O$(WR) in a pluton or co-genetic suites, even if minerals have constant $\delta^{18}O$, and why zircon best tracks magmatic $\delta^{18}O$.

Various approaches can be used to predict equilibrium fractionations ($\Delta^{18}O$) between igneous rocks, melts, and their various constituent minerals. Valley *et al.* (1994) used correlation of $\Delta^{18}O$(WR–Zrc) in four model rock compositions of varying SiO_2 content to derive an approximate

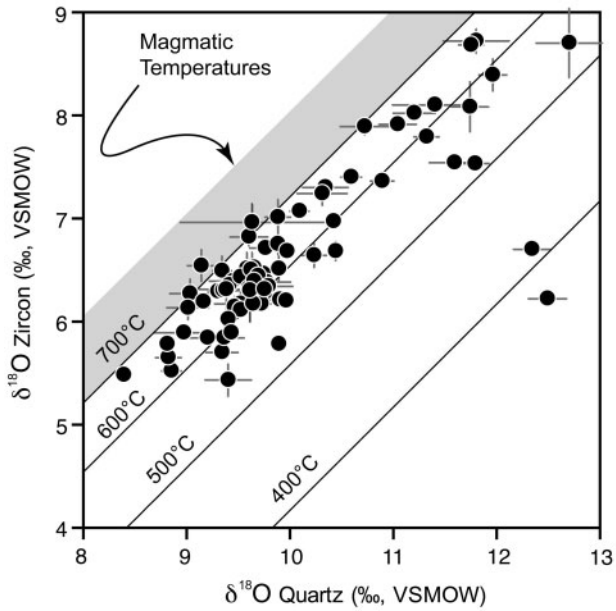

Fig. 7. δ–δ plot for quartz and zircon. Fractionations yield apparent temperatures that are lower than expected for high-temperature magmatic equilibrium. Isotherms calculated from Valley *et al.* (2003).

relationship of $\Delta^{18}O$(WR–Zrc) as a function of wt % SiO_2. By assuming all minerals were in equilibrium at 800°C, they calculated whole-rock $\delta^{18}O$ values that were mass balanced for the mode of each mineral in a rock. Two recent studies have used normative mineralogy to calculate $\Delta^{18}O$(melt–mineral) values (Appora *et al.*, 2003; Zhao & Zheng, 2003). This approach uses the principles of the Garlick Index (Garlick, 1966), which considers the degree of polymerization in a magma. Felsic magmas contain greater amounts of Al and Si, stabilizing minerals whose crystal chemistry favors stronger oxygen bonding, and therefore higher $^{18}O/^{16}O$ ratios. The disadvantage of using normative mineralogy includes omission of hydrous phases, poorly known fractionation factors for some normative phases, and mismatch between normative mineralogy and actual rock modes.

$\Delta^{18}O$(WR–Zrc) in the Sierra Nevada

Modeling of $\Delta^{18}O$(WR–Zrc) uses a compilation of 297 SNB rocks ranging from gabbro to granite that the US Geological Survey analyzed for mineral modes and SiO_2 (see Electronic Appendix 3). The silica content of each rock is directly related to $\Delta^{18}O$(WR–Zrc), which is calculated from the modal abundance and the equilibrium fractionation factors for quartz, K-feldspar, plagioclase, biotite, hornblende, and zircon (see 'Methods'). Solidus temperatures appropriate for magma compositions ranging from gabbro to high-silica granite were chosen (Fig. 8c), with the justification that both solidus and zircon saturation temperatures decrease with increasing SiO_2, such that $\Delta^{18}O$(WR–Zrc) represents different temperatures across a range of compositions. Recent Ti-in-zircon thermometry of a representative suite of these rocks confirms higher average Ti-in-zircon temperatures in diorites and gabbros than in peraluminous granites (Fu *et al.*, 2008). Solidus temperatures were assumed to have decreased linearly from 900°C (gabbro, $P_{H2O} = 3{\cdot}0$ kbar, 45 wt % SiO_2) to 650°C (high-silica granite, $P_{H2O} = 3{\cdot}0$ kbar, 78 wt % SiO_2). Calculated $\Delta^{18}O$(WR–Zrc) values show a strong ($r^2 = 0{\cdot}96$) positive correlation with SiO_2 (Fig. 8c). A linear fit yields the following equation:

$$\Delta^{18}O(\mathrm{WR-Zrc}) \approx 0{\cdot}0612(\text{wt \% } SiO_2) - 2{\cdot}50‰. \quad (1)$$

Equation (1) allows $\delta^{18}O$(WR) values to be calculated based on measured $\delta^{18}O$(Zrc) and whole-rock silica content. Possible sources of error on calculated $\delta^{18}O$ come from uncertainty in SiO_2 content and $\delta^{18}O$(Zrc). If SiO_2 and $\delta^{18}O$(Zrc) uncertainties are 0·5% and 0·1‰, respectively, the error on the calculated $\delta^{18}O$(WR) is ±0·12‰.

Comparison of measured and calculated $\delta^{18}O$(WR) values shows that many Sierran rocks deviate from the predicted values (Fig. 8d). To estimate the number of rocks that are hydrothermally altered, the average analytical precision (0·12‰, 1SD, Fig. 8d) of $\delta^{18}O$(WR) analyses was used as a cutoff. In cases where calculated and measured $\delta^{18}O$(WR) values vary by greater than ±0·12‰ of the calculated WR uncertainty and 3SD of analytical precision (>0·36‰), the $\delta^{18}O$(WR) is considered altered. By these criteria, approximately 28% of the $\delta^{18}O$(WR) values in the central Sierra are altered. Many values deviating by less than 0·36‰ are probably altered as well; thus 28% is a minimum estimate. Textural indicators of alteration include widespread sericitization of feldspar and chlorite and epidote veins and overgrowths.

Inspection of Fig. 8d shows that most of the measured $\delta^{18}O$ values showing alteration are higher than their expected magmatic value. Closed-system sub-solidus exchange in a rock will result in shifts in $\delta^{18}O$ among the minerals in a rock relative to one another, but the overall $\delta^{18}O$(WR) will remain unchanged. Alteration causing a shift in $\delta^{18}O$(WR) typically results from sub-solidus exchange with externally derived fluids, possibly at a wide range of temperatures and fluid compositions. The positive shift of $\delta^{18}O$(WR) observed for most samples is inconsistent with infiltration of meteoric water; however, three samples with low-$\delta^{18}O$(WR) values, 2–5‰, confirm some sub-solidus infiltration of heated meteoric water in the eastern Sierra (Fig. 8d). The samples come from areas of the eastern Sierra where igneous barometry indicates shallow (<2 kbar) depths of crystallization (Ague & Brimhall, 1988*a*; Ague, 1997). Hydrogen isotope data from these same areas confirm infiltration of meteoric water as δD(WR) values are commonly less than −85‰ (Godfrey, 1962; Masi *et al.*, 1981). In addition, samples from the

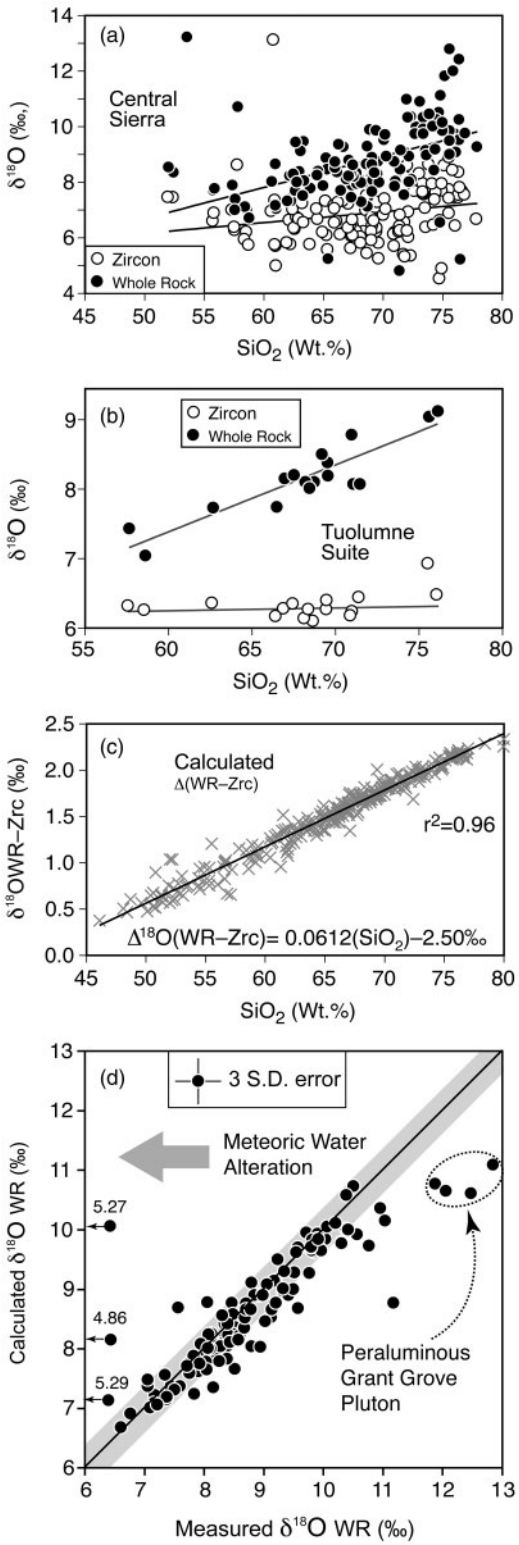

Fig. 8. Correlation of $\delta^{18}O$ and silica content. (a) $\delta^{18}O$(Zrc) and $\delta^{18}O$(WR) vs SiO_2 for all samples. (b) Pattern of $\delta^{18}O$(Zrc) and $\delta^{18}O$(WR) vs SiO_2 in the Tuolumne Intrusive Suite. Trends of fixed $\delta^{18}O$(Zrc) but increasing $\delta^{18}O$(WR) with SiO_2 should be noted. One anomalously high $\delta^{18}O$(Zrc) value was omitted from the linear best fit of the data. (c) Calculated $\delta^{18}O$(WR–Zrc) vs SiO_2 using a compilation of Sierran rocks with published SiO_2 and modal data (see Electronic Appendix 3). (d) Direct comparison of calculated and measured $\delta^{18}O$(WR). The grey field bounding the equilibrium line is 3SD of analytical uncertainty wide.

peraluminous Grant Grove pluton have measured $\delta^{18}O$(WR) values that are 1–2‰ greater than predicted (Fig. 8d). These samples are from the margin of the pluton and record contamination by high-$\delta^{18}O$ wall-rocks after zircon crystallized (Lackey *et al.*, 2006).

Although generally slight, alteration is enough to obscure isotopic zoning in plutons or intrusive suites and can hide detail such as $\delta^{18}O$ discontinuities. Figures 5a, b and 6a, b show direct comparison of measured and calculated $\delta^{18}O$(WR) across the SNB. In these two transects, additional calculated $\delta^{18}O$ values are shown, although they are less precise because SiO_2 was not measured for those samples and was estimated from published SiO_2 data (see Electronic Appendix 4). This direct comparison along transects shows local zones of alteration. For instance, the White Mountains have both low and variable measured $\delta^{18}O$, and calculated values that are higher and less variable, suggesting additional areas of meteoric water infiltration, one of which is confirmed below.

Two case studies distinguishing magmatic and alteration history

The Barcroft pluton

In the Jurassic Barcroft pluton, northern White Mountains (Fig. 3), pervasive secondary mineralization and a wide range of $\delta^{18}O$(WR) values (6–10‰) indicate hydrothermal alteration of the pluton (Ernst & Rumble, 2003). Three widely spaced zircon samples in the pluton show that magmatic $\delta^{18}O$ was in fact very homogeneous: 7·60‰ ± 0·08 (Fig. 9a). Using the zircon data from this study and measured SiO_2 of Ernst & Rumble (2003), magmatic $\delta^{18}O$(WR) is calculated to vary less than 1‰ in the pluton. All measured $\delta^{18}O$(WR) values deviate over 1‰ from calculated values, and three of four measured values are lower than calculated (Fig. 9a). Although none of the $\delta^{18}O$(WR) values that Ernst & Rumble (2003) reported is exceptionally low, the tendency toward lower measured values confirms some meteoric water infiltration during hydrothermal alteration of the Barcroft pluton.

Saddlebag Lake meta-rhyolite

A Triassic rhyolite in the Saddlebag Lake pendant, east of the Tuolumne Suite (Fig. 3), has a complex magmatic, alteration, and metamorphic history. The rhyolite has a typical $\delta^{18}O$(Zrc) value of 6·2‰. In contrast, the $\delta^{18}O$ values of the whole-rock and quartz phenocrysts are 11·6‰ and 12·6‰, respectively; both are elevated well above typical igneous values and confirm alteration (Fig. 9b). If the original SiO_2 content of the rhyolite was

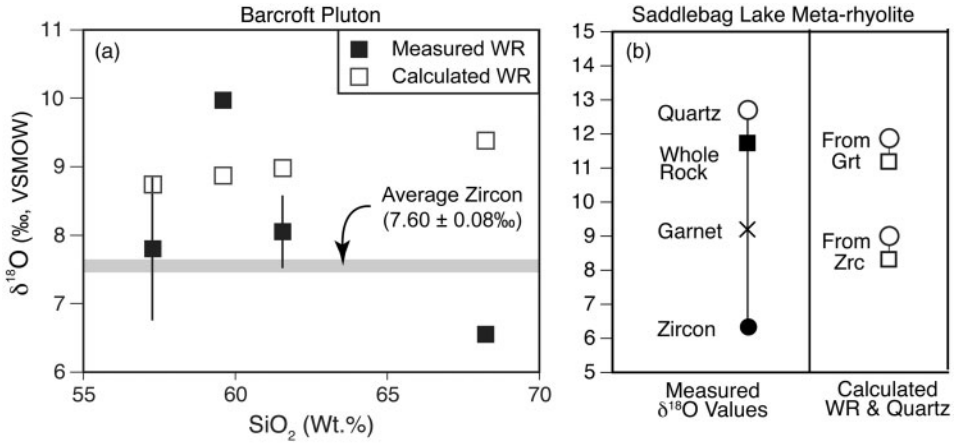

Fig. 9. Alteration in the Barcroft pluton and Saddlebag Lake meta-rhyolite. (a) SiO_2 vs $\delta^{18}O$ of zircon and whole-rock (measured and calculated) values in the Jurassic Barcroft pluton. The small range of $\delta^{18}O$(Zrc) and calculated $\delta^{18}O$(WR) relative to measured values should be noted. Barcroft $\delta^{18}O$(WR) and SiO_2 values from Ernst & Rumble (2003). (b) $\delta^{18}O$ of quartz and whole-rock in the Saddlebag Lake meta-rhyolite are altered and higher than expected according to $\delta^{18}O$(Zrc). Disequilibrium $\delta^{18}O$ between metamorphic garnet and zircon indicates that garnet crystallized after alteration. Calculated whole-rock and quartz $\delta^{18}O$ relative to both garnet and zircon emphasize systematic differences between the meta-rhyolite and its precursor.

70 wt %, then the calculated $\delta^{18}O$(WR) is *c.* 8·3‰ (Fig. 9b), much lower than the measured value.

Metamorphic garnet in the meta-rhyolite yields another constraint on its alteration history. Because garnet has slow oxygen diffusion (Couglan, 1990; Vielzeuf *et al.*, 2005), like zircon, it records the $\delta^{18}O$ of a rock at the time it crystallizes. For Fe–Mn garnets, equilibrium fractionation with zircon is ~0‰ at magmatic temperatures (Valley *et al.*, 2003). Therefore, the 9‰ garnet is not equilibrated with the 6·2‰ zircon. As such, a chronology of events affecting the rhyolite is: (1) the rhyolite was erupted; (2) hydrothermal alteration elevated $\delta^{18}O$(WR); (3) Cretaceous metamorphism of the altered rhyolite led to garnet crystallization and re-equilibration of all phenocrysts except zircon.

Regional $\delta^{18}O$ belts

Zone 1: Foothills belt

Mantle-like $\delta^{18}O$(Zrc) values occur in and around mafic ring dike complexes in the western Sierran foothills (Fig. 4, inset). This low-$\delta^{18}O$ domain abruptly changes to high-$\delta^{18}O$ rocks 20 km into the batholith (Fig. 5a). The extent of interaction between basement rock and magmas in this belt is unclear, although detailed O, Sr, and Nd isotope investigation of the ring dike complexes indicates a nonradiogenic, depleted mantle source with melting at pluton–wall-rock contacts causing some localized contamination (Clemens-Knott, 1992). Mantle-like $\delta^{18}O$(Zrc) values appear to rule out widespread contamination; however, the average $\delta^{18}O$(WR) of the wall-rocks, a mélange of the Kings–Kaweah ophiolite belt (Saleeby, 1992; Saleeby & Busby, 1993), is 7·1 ±1·3‰ (Lackey *et al.*, 2006). Thus, there is minimal magma–wall-rock isotopic contrast, which would obscure source or contamination contributions from melting of ophiolitic rocks.

Zone 2: Fine Gold–Sequoia belt

In the Fine Gold Suite $\delta^{18}O$ decreases from west to east, and is negatively correlated with Sr_i (Figs 4 and 6a); rocks with high $\delta^{18}O$(Zrc), up to 8·7‰, have low Sr_i (~0·704). The pattern of these isotope ratios requires substantial input of hydrothermally altered ocean crust or volcanic arc sediments in the western parts of the Fine Gold suite (e.g. Fig. 2a). In ocean crust, circulation of heated water increases the $\delta^{18}O$(WR) of upper pillow basalt and sheeted dike sections considerably from mantle values (altered ~10‰, unaltered 5·4–6·0‰; McCulloch *et al.*, 1980; Muehlenbachs, 1998). Low Sr_i values result because $^{87}Sr/^{86}Sr$ is only modestly elevated from mantle values by alteration (McCulloch *et al.*, 1980; Muehlenbachs, 1998). Furthermore, low Sr_i indicates that the rocks are relatively young because insufficient time has passed for significant ingrowth of ^{87}Sr. Similar $\delta^{18}O$ and Sr_i would be expected for arc volcanic rocks, such as greywacke, that have been hydrothermally altered (Magaritz & Taylor, 1976).

East of the Fine Gold rocks, $\delta^{18}O$ and Sr_i show positive correlation in a series of plutons that lead up to the PA/NA break (Figs 3 and 6). In the Fresno Sheet, rocks of Zone 2 initially have high $\delta^{18}O$ and sub-0·706 Sr_i values (Fig. 5; 38–55 km), indicating sources with juvenile supracrustal rock, but less than the Fine Gold Suite. Eastward increasing $\delta^{18}O$ and Sr_i in the belt, into the Sequoia region, mimics the pattern in plutons east of the Fine Gold Suite, with the PA/NA break again marking the transition to lower $\delta^{18}O$.

Overall, the geochemistry of the plutons in Zone 2 reflects the influence of the exposed wall-rocks. For instance, rocks of the Fine Gold Suite with the highest $\delta^{18}O$ are in direct contact with volcaniclastic rocks of the

Jurassic–Triassic island arc belt and outboard accretionary sequence of the Sierran foothills (Fig. 4; Snow & Scherer, 2006). These rocks have the exact isotopic composition, with low Sr_i (0·704–0·707; Kistler & Peterman, 1973) and high $\delta^{18}O$(WR) (8–14‰; Böhlke & Kistler, 1986), to produce the local contamination patterns in the Fine Gold Suite. Negative correspondence of Sr_i and $\delta^{18}O$ on the east side of the Fine Gold Suite suggests differences of magma source and contamination (Fig. 6). Permo-Triassic chert–argillite mélange of the Calaveras Complex is in fault contact with the Jurassic–Triassic metamorphic rocks belt near the 0·706 line (Fig. 4). Pendants and septa show southeastern continuation of both metamorphic belts to their termination near the boundary of the Mariposa and Fresno sheets (Fig. 4). Therefore the Bass Lake Tonalite intrudes across the fault contact into both metamorphic belts. Because Calaveras rocks contain greater amounts of continental sediments than rocks to the west, eastward increases of Sr_i in the Bass Lake Tonalite indicate greater proportions of Calaveras Complex rock in magma sources or as a contaminant (Fig. 6a and b). Decreasing $\delta^{18}O$ may reflect greater depleted mantle contributions to the east or lower degrees of partial melting of refractory chert and argillite-rich Calaveras rocks. Minor partial melting, especially involving labile phases such as micas, can radically shift magmatic Sr_i without markedly changing $\delta^{18}O$. Thus, the 0·706 line may reflect crustal architecture as well as wall-rock fertility.

Another example of wall-rock influence on magma chemistry in the Zone 2 high-$\delta^{18}O$ belt concerns the Kings Sequence, which contaminates magmas throughout the Sequoia region (Fig. 4; Ague & Brimhall, 1988*b*; Kistler, 1990; Chen & Tilton, 1991). Kings Sequence rocks and some from the Calaveras Complex host the Strongly Contaminated and Reduced plutons of Ague & Brimhall (1988*b*). These plutons, including several that are peraluminous (Fig. 3), intrude Kings Sequence rocks (Fig. 3). Ague & Brimhall (1988*b*) showed increased Fe/(Fe + Mg) in biotite in these rocks and proposed that graphite-rich Kings Sequence rocks led to magmas being relatively reduced, 0–2 log fO_2 units below QFM (quartz–fayalite–magnetite). High $\delta^{18}O(Zrc) > 7{\cdot}5‰$, but relatively low Sr_i (0·704–0·707), in these plutons shows that they contain high proportions of young supracrustal rocks in their sources; comparison of pluton margin and interior geochemistry and mineralogy reveals localized melting and contamination by the Kings Sequence (Lackey *et al.*, 2006).

Zone 3: Sierra Crest and eastern Sierra

East of Zones 1 and 2 there is a monotonic decrease in $\delta^{18}O$ toward the Sierra Crest (Fig. 5, 55–104 km; Fig. 6, 85–130 km). Many of the values in the eastern Sierra fall in the range of mantle $\delta^{18}O(Zrc)$ values (5·3 ± 0·3‰, Valley *et al.*, 1998). Calculated $\delta^{18}O$(WR) values for granodiorites and granites in this belt are 7–8‰. These relatively low values agree with studies proposing that significant portions of the late Cretaceous SNB were generated directly from melting of enriched ($Sr_i = 0{\cdot}706$; $\varepsilon Nd = -4{\cdot}5$) lithospheric mantle beneath the eastern Sierra (Coleman *et al.*, 1992; Coleman & Glazner, 1997). Although pendants of metavolcanic and metasedimentary rock are exposed in the eastern Sierra (Fig. 3), $\delta^{18}O$ values do not indicate significant magmatic incorporation of these or other crustal rocks.

Zone 4: Owens Valley–White Mts. belt

Triassic, Jurassic, and Cretaceous plutons in the Owens Valley, Long Valley re-entrant, and White Mountains typically have $\delta^{18}O(Zrc) > 6{\cdot}5‰$ (Fig. 4). Values of Sr_i in these rocks often exceed > 0·709 (Fig. 6c), indicating magma sources containing aged sediments or crust. Wall-rock contamination effects are pronounced in many of the solitary plutons in the White Mountains that intrude Proterozoic to Paleozoic continental-derived sedimentary rocks. Values of Sr_i and εNd at the margin and cupola regions of the plutons are more crustally influenced ($Sr_i > 0{\cdot}710$, $\varepsilon Nd < -9{\cdot}0$) than their interiors ($Sr_i < 0{\cdot}706$, $\varepsilon Nd > -1{\cdot}5$; Ernst *et al.*, 2003), indicating 'veneers' of contamination.

Crustal boundaries

Projection of lateral changes of $\delta^{18}O$ in the SNB shows mostly gradual changes (Figs 5 and 6); however, localized, sharp, step-function changes of $\delta^{18}O$ suggest steeply dipping trans-crustal breaks. Abrupt lateral shifts in $\delta^{18}O$ suggest that magmas generated on either side of a break inherit the $\delta^{18}O$ signature of the terrane in which they form, with a steep geometry of the terrane boundary preventing significant averaging of values across the break (see Peck *et al.*, 2004). Below we discuss two significant lithospheric breaks that are resolved by $\delta^{18}O(Zrc)$, and the position of the PA/NA break.

Foothills Break

The abrupt increase of 1·5‰ in $\delta^{18}O(Zrc)$ that separates Zones 1 and 2 in the western Fresno sheet (20 km, Fig. 5a), is not discernible from $\delta^{18}O$(WR) or Sr_i (Fig. 5), but may be the geochemical expression of the Foothills suture (Saleeby, 1992), which is poorly exposed. Saleeby (1992) proposed northward projection of the Foothills suture into the Bass Lake Tonalite, but the limited extent of Zone 1 low-$\delta^{18}O$ rocks to the north means that the break terminates before the tonalite. Greater wall-rock heterogeneity to the north and different magmatic style may conceal the break.

Eastern Sierra Break

The sharp 1‰ west-to-east increase of $\delta^{18}O(Zrc)$ defining the boundary between Zones 3 and 4 (Figs 4 and 6a, 128 km), defines a feature in the eastern Sierra and Owens and Long Valleys that has long been inferred to be a major

crustal boundary (Saleeby *et al.*, 1986; Kistler, 1993). This discontinuity corresponds to Intrabatholithic Break 3 (IBB3) of Saleeby *et al.* (1986), and the Tinemaha Fault of Stevens *et al.* (1997). This boundary was originally recognized by displacement of Jurassic and Triassic rocks along a lineament that intersects a major right-lateral offset in the 0·706 line in Long Valley (Fig. 4). The boundary is also inferred from structural and stratigraphic relationships where SW-trending Neoproterozoic to Triassic sedimentary shelf sequences in the White–Inyo Mountains are juxtaposed against the NW-trending SNB (Stevens *et al.*, 1997). A steeply dipping geometry for this break favors tectonic truncation as the mode of origin, and the expression of the $\delta^{18}O$ step in Triassic and younger plutons means that the boundary is at least pre-Jurassic. In addition, recent dating of dikes offset in the Owens Valley indicates that the 65 km of dextral offset along this break occurred since 83 Ma (Kylander-Clark *et al.*, 2005).

PA/NA Break

Values of $\delta^{18}O$(Zrc) decrease gradually at the PA/NA break (Figs 5a and 6a) and generally correspond to its originally proposed location (Fig. 4). The lack of a sharp step in $\delta^{18}O$ suggests a diffuse transition, rather than a trans-crustal break; yet changes in isotopic gradients, and the preponderance of data from the high- to low-$\delta^{18}O$ zones that define it, indicate that this is a major lithospheric discontinuity. Potentially, the integrated effects of lithospheric mantle differences as well as an upper crustal overprint have blurred the break; however, such complex controls cannot be evaluated with certainty. Although the PA/NA break remains enigmatic, $\delta^{18}O$(Zrc) values show that some adjustments of the position of the PA/NA break are needed.

In the Fresno sheet, we propose two refinements. First, the trace of the break appears to be west of the Mineral King pendant, rather than through it (Fig. 4). Whereas Kistler (1993) proposed linking the PA/NA break to faults in the Mineral King pendant, the low $\delta^{18}O$(Zrc) of the pluton to the west of the pendant (granodiorite of Castle Creek) suggests that the break is ~10 km to the west (Fig. 4). Whereas the Mineral King pendant has lithologies similar to the Kings Sequence, volcanic rocks in the pendant have affinities with eastern terranes (Saleeby & Busby, 1993). The second adjustment is a 5 km eastward shift of the break at the Boyden Cave pendant (Fig. 4). The pendant clearly juxtaposes rocks from the Kings Sequence and the Goddard terrane to the east; however, refinement based on $\delta^{18}O$ may better reflect the deep orientation.

North of the Mount Givens pluton, in the Mariposa sheet, the original PA/NA break strikes NW and joins the 0·706 line; however, high- and low-$\delta^{18}O$ domains are continuously juxtaposed to the north (Fig. 4). If the bulbous westward protrusions of the Mount Givens pluton and Tuolumne Intrusive Suite are ignored as distortional effects (Fig. 4), the $\delta^{18}O$-defined PA/NA break projects directly through Yosemite to the offset 0·706 line in the Sonora Intrusive Suite (Fig. 4). Whereas Kistler (1993) favored the joining of the PA/NA break and 0·706 line to include the Melones fault as a northern extension of the PA/NA break, Seleeby *et al.* (1986) proposed that a straight intrabatholithic break, labeled IBB2 in Fig. 4, continues from the PA/NA trace into Yosemite (Kistler, 1993). The pattern of $\delta^{18}O$ supports the northward trend into Yosemite.

Direct comparison of O, Sr, and Pb isotopes

Chen & Tilton (1991) reported Sr and Pb isotope ratios on a subset of samples analyzed in this study from the Fresno sheet (see Chen samples in Fig. 3). Therefore, correlation of O, Sr, and Pb isotope ratios can be evaluated for a representative suite of rocks across the SNB (Fig. 10). Plots depict Sr and Pb isotope variation relative to $\delta^{18}O$ of zircon (Fig. 10a–d) and whole-rocks (Fig. 10e–h) to evaluate the effect of differing silica among samples on isotopic correspondence. The samples are divided into western and eastern samples; western samples have $Sr_i < 0{\cdot}706$; eastern samples occur east of the PA/NA break. A third group of samples are from the Sequoia region (Fig. 3).

Oxygen and strontium isotopes

Co-variation of $\delta^{18}O$(Zrc) with Sr_i is geographically distinct for the western and eastern Sierra (Fig. 10a). Calculated $\delta^{18}O$(WR) comparisons yield more scatter but similar trends (Fig. 10e). The array of $\delta^{18}O$ and Sr_i for western samples intersects a mantle value at the low-Sr_i end (Clemens-Knott, 1992) and trends toward an evolved (high-Sr_i) reservoir; overall there is resemblance to the Peninsular Ranges trend (e.g. Fig. 2b). One sample from the margin of the Grant Grove pluton lies well off the western trend, recording contamination typical of the Sequoia region (Fig. 10a).

Eastern samples also exhibit a distinct correlation, with a less steep positive slope, forming a flat array of high Sr_i values throughout the eastern Sierra. Both low- and high-$\delta^{18}O$ plutons indicate considerable heterogeneity in the crustal content of these magmas, with low $\delta^{18}O$ values reflecting old lithospheric mantle (e.g. Coleman & Glazner, 1997); high $\delta^{18}O$ values record melting of crust with variable proportions of supracrustal-derived rock.

Sequoia region rocks have distinctly higher Sr_i values relative to the eastern and western series, but the data are more scattered (Fig. 10a). The variable $\delta^{18}O$ and Sr_i of this sample group exemplifies the widespread but heterogeneous contamination by the Kings Sequence.

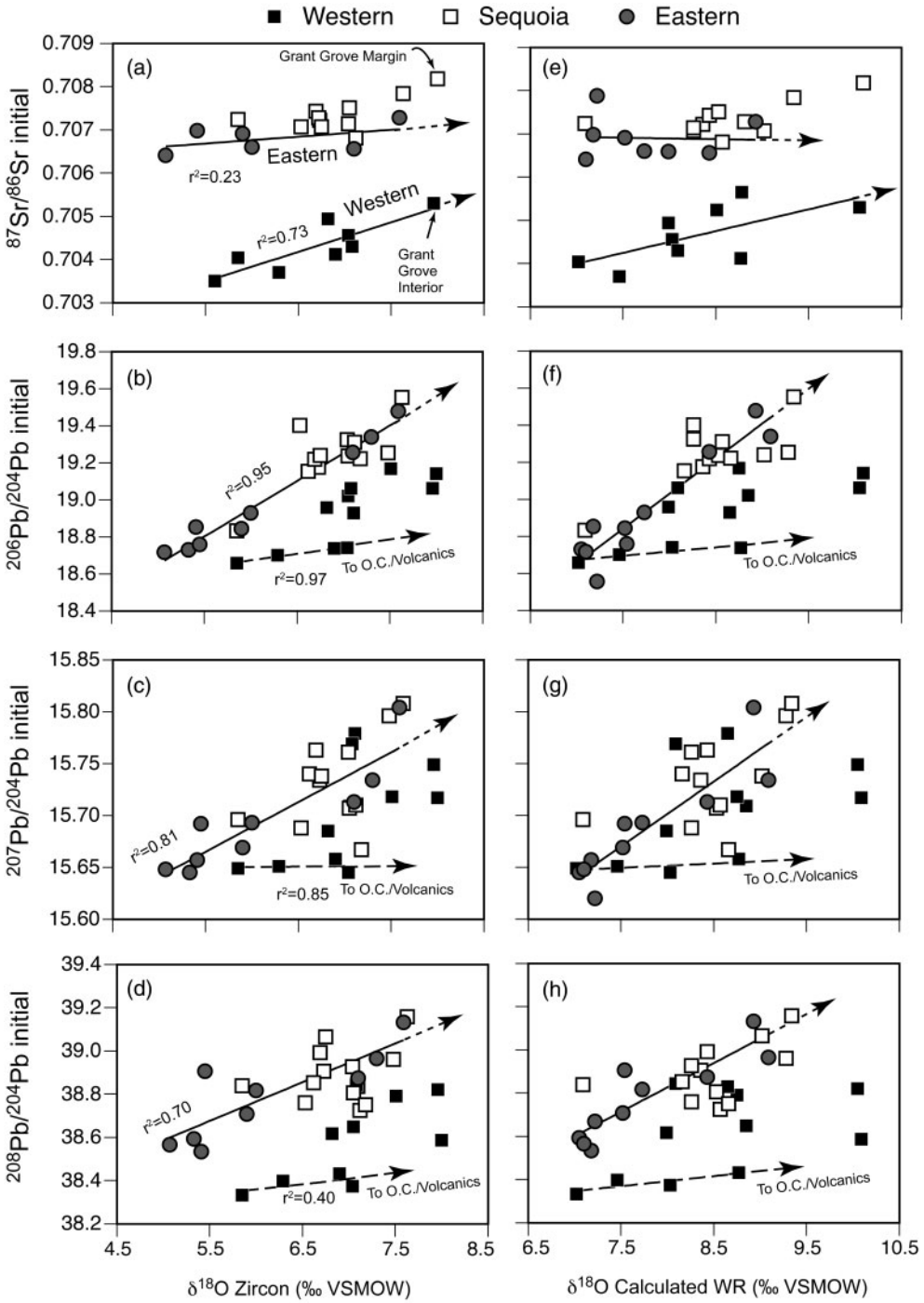

Fig. 10. Correspondence of $\delta^{18}O$ to Sr and Pb isotope ratios across the Fresno sheet. (a) $\delta^{18}O$(Zrc) vs $^{87}Sr/^{86}Sr$ initial. (b–d) $\delta^{18}O$(Zrc) vs initial Pb isotope ratios. (e) $\delta^{18}O$ calculated whole-rock (WR) vs $^{87}Sr/^{86}Sr$ initial. (f–h) $\delta^{18}O$ calculated WR vs initial Pb isotope ratios. Trend lines represent least-squares best fits to the data. The high-Sr_i sample from the contaminated margin of the Grant Grove pluton was omitted from the best fit of western samples; Sequoia samples were not fitted with a trendline because of overall poor correlation.

Oxygen and lead isotopes

Lead isotope ratios positively correlate with $\delta^{18}O$(Zrc) and western and eastern trends are distinct (Figs 10b–d). Calculated whole-rock $\delta^{18}O$ again shows more scatter, but, nevertheless, consistent patterns (Figs 10f–h). All initial Pb isotope ratios ($^{206}Pb/^{204}Pb$; $^{207}Pb/^{204}Pb$; $^{208}Pb/^{204}Pb$) become more radiogenic with increasing $\delta^{18}O$(Zrc). The lowest $\delta^{18}O$ values of both eastern and

western samples tend to have similar initial $^{206}Pb/^{204}Pb$ and $^{207}Pb/^{204}Pb$, close to the primitive mantle value at 100 Ma (Chen & Tilton, 1991). Chen & Tilton (1991) suggested that eastern samples have higher $^{208}Pb/^{204}Pb$ because U/Pb was lower than Th/Pb in the source rocks, an indication of preferential extraction of U by fluid escape during granulite-facies metamorphism.

The increasing variability of initial Pb isotope composition with $\delta^{18}O$ in western samples produces a 'fan-like' spread of the data, which suggests a common low-$\delta^{18}O$ mantle reservoir input (Fig. 10b–d), but highlights source or contamination complexity in high-$\delta^{18}O$ rocks that is not evident from Sr_i (Fig. 10a). Most western samples document input of aged crust or sediments thereof; however, a group of four samples from the westernmost rocks change little in initial Pb, whereas $\delta^{18}O$(Zrc) ranges from 6·0 to 7·0‰; these same samples trend toward increasing Sr_i (Fig. 10a). Not surprisingly, the O–Pb–Sr systematics of these samples are consistent with incorporation of altered ocean crust or arc volcanic rocks. Elevated Sr_i values but low initial Pb values show decoupling of these radiogenic isotope systems during supracrustal alteration of the source rocks.

Sequoia samples are also scattered with respect to $^{207}Pb/^{204}Pb$ and $^{208}Pb/^{204}Pb$ (Fig. 10c and d); $^{207}Pb/^{204}Pb$ values overlap considerably with those for western and eastern rocks (Fig. 10c). The highly variable $\delta^{18}O$–Pb pattern, and the fact that many samples fall between the western and eastern trends, suggests a diverse source and contamination history for this group of plutons.

Large-scale magma systems

Positive correlation of O, Pb, and Sr isotopes indicates both mantle and crustal inputs in the western and eastern Sierra magmas. Each sample defining these trends is a complex integration of source characteristics and contamination, magma mixing, differentiation, and assimilation, obscuring the origin. Nevertheless, correlations for eastern SNB samples are reasonably strong in most cases and distinct in slope from western SNB rocks. This is a remarkable pattern considering that samples in each group vary considerably in age, up to several million years, and location within their respective domains (Fig. 3). Therefore, we hypothesize that two distinct magma systems operated.

It is widely acknowledged that different 'styles' of magmatism occur in the western and eastern Sierra (e.g. Chen & Tilton, 1991; Coleman & Glazner, 1997; Tikoff & de Saint Blanquat, 1997; Wenner & Coleman, 2004), and the Peninsular Ranges batholith bears some similarity (Gromet & Silver, 1987; Tulloch & Kimbrough, 2003; Lee *et al.*, 2007). The isotopic patterns imply unique controls on isotope ratios on each side of the batholith that permitted largely continuous trans-batholith gradients in major and minor element chemistry (e.g. Bateman, 1992).

Differing lithosphere compositions in the SNB undoubtedly provide a major control on the isotopic composition of the magmas (Kistler, 1990); yet to average out heterogeneity of crust and mantle reservoirs and produce well-defined isotopic trends requires a long-lived and stable source region, such as is envisaged by the melting, assimilation, storage, and homogenization (MASH) model of Hildreth & Moorbath (1988). Ducea (2001, 2002) and Saleeby *et al.* (2003) adopted the MASH model to explain magmatic averaging that results in complementary geochemistry between batholithic crust and xenoliths thought to represent residues of melting at the base of the arc crust. Annen *et al.* (2006) proposed the existence of deep crustal 'hot zones' beneath large magma systems in which the geochemical character of the magmas is largely imparted in the source but textural diversity is acquired in the crust during crystallization. Clearly, other models may be applicable, but the MASH and 'hot zone' models are apt in that they permit large-scale magma systems that could support long-term geochemical connectivity, but allow for progressive emplacement of texturally diverse plutons.

In addition to basement composition effects, the two magma systems probably varied in depth of melting. In particular, eastern Sierra $\delta^{18}O$ values indicate mostly mantle sources. This finding concurs with a growing consensus of studies invoking direct melting of the lithospheric mantle and remelting of underplated juvenile magmas as the origin of most magmas in the eastern Sierra (Coleman & Glazner, 1997; Wenner & Coleman, 2004; Ratajeski *et al.*, 2005; Sisson *et al.*, 2005). Broadly characterized, this magma system was driven by massive infracrustal recycling at a deep locus of melting. Any crustal melting that did happen would involve lower crust composed of orthogneiss or amphibolite metamorphosed to granulite facies (Chen & Tilton, 1991); increases of $\delta^{18}O$ from melting of such rocks would be minimal (Kistler, 1990).

Except for the Foothills belt, which represents the nascent stages of magmatism in the Sierran arc, greater crustal melting, recycling, and contamination, including abundant melting of supracrustal rocks, defines the western magma system. The high-$\delta^{18}O$ magmas of the Fine Gold–Sequoia belt, and evidence of wall-rock controls on $\delta^{18}O$ are consistent with a shallow locus of magma generation that melted and reworked the crust considerably. The high content of greywacke and hydrous, disaggregated ophiolite lithologies present in the basement rocks of the western Sierra potentially proved more fertile for melting and facilitated recycling (Montel & Vielzeuf, 1997; Vielzeuf & Schmidt, 2001).

Small-scale magma systems: plutons and intrusive suites

Beyond evidence for two large-scale magmatic domains in the SNB, we observe intriguing spatial and temporal patterns of $\delta^{18}O$ variation within intrusive suites and

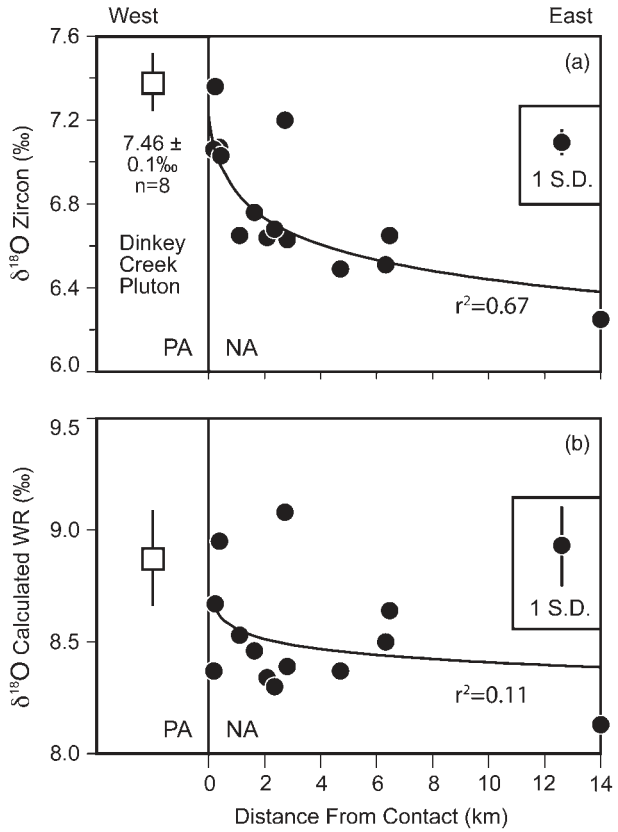

Fig. 11. Variation of $\delta^{18}O$(Zrc) in the Mount Givens pluton. (a) Increasing $\delta^{18}O$ toward the western margin of the pluton approaches values of the Dinkey Creek Granodiorite across the PA/NA break. (b) Calculated $\delta^{18}O$(WR) values poorly resolve $\delta^{18}O$ zoning because SiO_2 content varies considerably in the pluton; curve fits are power law.

individual plutons. Examples of these smaller-scale systems are discussed below and we evaluate the causes of their isotopic diversity and implications for magma sources, contamination, and batholith construction.

Mount Givens Granodiorite

The Mount Givens Granodiorite exhibits a gradual 1‰ increase in $\delta^{18}O$(Zrc) on its west side (Fig. 11a) where the pluton abuts the older Dinkey Creek Granodiorite (102 Ma, Tobisch *et al.*, 1995) at the PA/NA boundary (Fig. 6a). Compared with zircon, the calculated $\delta^{18}O$(WR) blurs this pattern because inward changes in lithology from a tonalitic margin to a granitic interior result in highly variable calculated $\delta^{18}O$(WR) values (Fig. 11b). Because textures and mineral proportions vary considerably (Bateman, 1992; McNulty *et al.*, 2000), as does the range of U–Pb zircon ages (87·9–92·8 Ma), the pluton appears to be constructed by multistage growth (McNulty *et al.*, 2000). The trend of $\delta^{18}O$(Zrc) suggests that the western margin of the pluton has a geochemical affinity with the PA domain, whereas the $\delta^{18}O$ of the younger eastern areas reflects the NA domain. Similarly, the Eagle Peak pluton, just to the west of the Mount Givens pluton (Fig. 4), shows zoning in O, Sr, and Nd isotopes that hints at variable contamination of the magma as it ascended along the PA/NA break (Hill *et al.*, 1988).

Sequoia Intrusive Suite

The Sequoia Intrusive Suite (Fig. 3) exhibits distinct $\delta^{18}O$ zonation. The outer and largest pluton, the Giant Forest Granodiorite, has the highest $\delta^{18}O$(Zrc) values of the suite and greater overall variation in $\delta^{18}O$; the interior granites of Big Meadows and Weaver Lake have lower average $\delta^{18}O$ values that are less variable (Fig. 12a). Average Sr_i also decreases inward in the suite: Giant Forest = 0·70799 ± 0·00204, $n = 6$; Big Meadows = 0·70733 ± 0·00011, $n = 2$; Weaver Lake = 0·70657 ± 0·00032, $n = 4$ (Chen & Tilton, 1991; Wenner & Coleman, 2004). Thus, the margin of the suite exhibits greater supracrustal contamination. In detail, samples from the Giant Forest Granodiorite have higher $\delta^{18}O$ in the southern half of the pluton where it abuts the Kings Sequence rocks of the Sequoia pendant (Fig. 3, Table 1). Such localized effects indicate upper crustal contamination and explain the $\delta^{18}O$ heterogeneity in the pluton. The Giant Forest pluton appears to have shielded the 'core' of the suite from contamination. Therefore, the lower isotope ratios of the interior plutons better represent the suite's source composition.

Sierra Crest Suites

Evolution of magmatic $\delta^{18}O$(Zrc) from oldest to youngest units is apparent in some plutonic suites exposed in the Sierra Crest (Fig. 12b–d). Relatively constant $\delta^{18}O$(Zrc) values occur in the Tuolumne Intrusive Suite (Fig. 12b), but others show progressive $\delta^{18}O$ changes (e.g. Sonora, John Muir, Fig. 12c and d). In addition, $\delta^{18}O$ is often homogeneous within each pluton of a suite, but varies between plutons.

The John Muir Suite

Plutons of the John Muir Suite (JMS, Fig. 3) display intriguing spatial and temporal trends of $\delta^{18}O$(Zrc). A subset of the JMS, the Mono Pass Suite, is approximately coeval with the Tuolumne Intrusive Suite, and includes, from oldest (95·3 Ma) to youngest (87·0 Ma), the gabbro of Rock Creek, Lake Edison Granodiorite, Round Valley Peak Granodiorite, and Mono Creek Granite (Gaschnig *et al.*, 2006). The Lamarck Granodiorite (94–92 Ma, J. Gracely, personal communication) and the Evolution Basin Alaskite (94–92 Ma, Wenner & Coleman, 2004) are exposed to the south of the Mono Pass Suite, and a new U–Pb zircon age for the Inconsolable Granodiorite (95 Ma, J. Gracely, personal communication) suggests that it may be a low-silica end-member of the southern JMS.

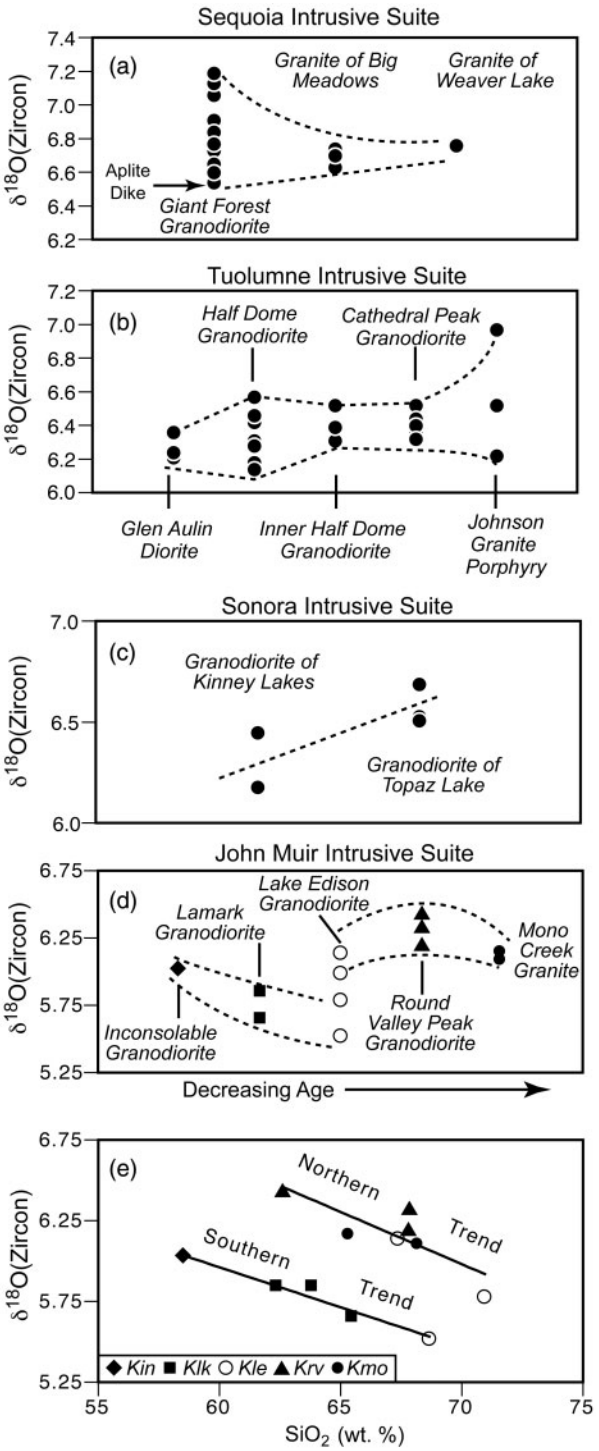

Fig. 12. $\delta^{18}O$(Zrc) of intrusive suites. (a) Sequoia Suite rocks show less variability in younger, interior members. (b) The Tuolumne Suite shows variation in $\delta^{18}O$ among members, but the average $\delta^{18}O$ is relatively constant. (c) $\delta^{18}O$ increases inward in Sonora Suite rocks. (d) John Muir Suite plutons show complex patterns of $\delta^{18}O$ with decreasing age. (e) Variation of $\delta^{18}O$ vs SiO_2 in Muir Suite rocks shows distinct northern and southern trends. Kin, Inconsolable Granodiorite; Klk, Lamark Granodiorite; Kle, Lake Edison Granodiorite; Krv, RoundValley Peak Granodiorite; Kmo, Mono Creek Granite.

Values of $\delta^{18}O$(Zrc) are reported for all the plutons of the JMS except the Rock Creek gabbro and Evolution Basin Alaskite (Table 1). Relative to pluton age, $\delta^{18}O$(Zrc) decreases with age in the two oldest plutons. It displays considerable variation in the Lake Edison pluton; $\delta^{18}O$(Zrc) is highest in the Round Valley Peak Granodiorite, and decreases in the Mono Creek Granite (Fig. 12d). Except for the Lake Edison Granodiorite, most plutons are relatively homogeneous in $\delta^{18}O$. Variation of $\delta^{18}O$ vs SiO_2 for John Muir samples also reveals two parallel trends of decreasing $\delta^{18}O$ with increasing SiO_2 (Fig. 12e). One trend, the 'southern trend' is defined by the two southern plutons (Inconsolable and Lamarck), whereas the Round Valley Peak, Mono Creek, and some of the Lake Edison samples define the 'northern trend'.

To explain the offset $\delta^{18}O$ trends in the JMS, we propose that the southern and northern trend plutons were produced from two distinct sources. The Lake Edison Granodiorite, with its wide range of $\delta^{18}O$, suggests a hybrid pluton produced by mixing between the two sources. Such behavior supports models for magma mixing as the origin of some granodiorites in the Sierra Nevada (Sisson *et al.*, 1996; Wenner & Coleman, 2004). In addition, higher $\delta^{18}O$ in the older plutons indicates that the early formed magmas contained higher proportions of recycled supracrustal rocks than later magmas. Decreasing $\delta^{18}O$ in the younger plutons is consistent with exhaustion of fusible crustal rocks in the magma sources, increased mantle contributions, or possibly conditioning of magma conduits (Scoates & Frost, 1996).

Temporal patterns of $\delta^{18}O$

Considering changes in $\delta^{18}O$(Zrc) over time for all rocks gives a more complete sense of the evolving arc magma system (Fig. 13a). In addition, magma production rates deduced from measurement of pluton area (Fig. 13b) reveal that the Cretaceous magma system experienced several episodic magma 'pulses'. These pulses are resolved at finer time-scales than the magmatic 'flare-ups' of Ducea (2001), and they correspond to changes in $\delta^{18}O$.

The first magmatic pulse, marked by increasing $\delta^{18}O$, resembles the Peninsular Ranges trend, and shows more supracrustal input with time. This period includes the transition from magmatism in the Foothills belt to the Fine Gold Suite and western Sequoia region. Subsequent pulses at 103–102 Ma and 99–97 Ma in the western and axial potions of the SNB saw widening of the range of $\delta^{18}O$ to both higher and lower values. A temporary decrease in magma production at around 95 Ma (Fig. 13b) led to voluminous magmatism in the eastern SNB. The pronounced downward shift of $\delta^{18}O$(Zrc) emphasizes the difference of the eastern Sierra magma system.

In arc settings, magmatism, heat flow, and development of MASH domains or 'hot zones' should facilitate greater crustal recycling with time. A secular change to increased

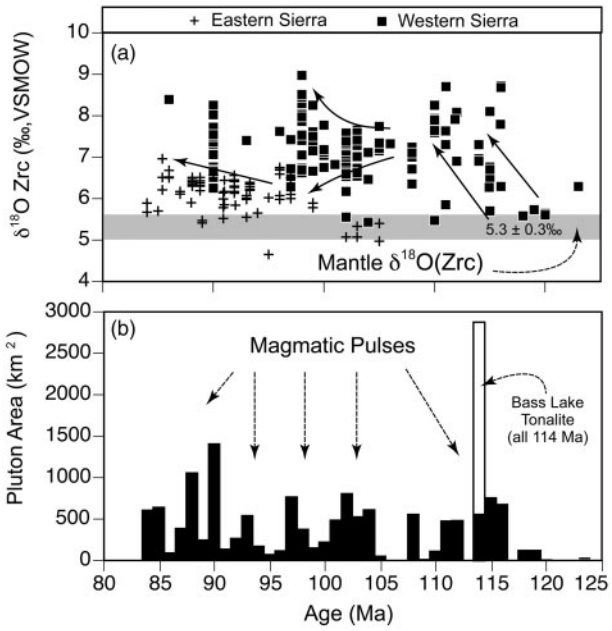

Fig. 13. Temporal variation of $\delta^{18}O$(Zrc) (a) and pluton area (b) in the central Sierra from 125 to 80 Ma. Gradients of $\delta^{18}O$ in (a) are discontinuous between different pulses of magmatism. The Bass Lake Tonalite can be subdivided according to the ages of lobes within the body (105–116 Ma; Stern *et al.*, 1981), or a single age of 114 Ma may be assigned (Bateman, 1992). The Sonora Intrusive Suite is not included in area calculations because incomplete mapping and geochronology west of the suite prevents estimation of the full intrusive area across that part of the batholith. Image analysis was employed to calculate the area of individual plutons that have been dated, including some that were not analyzed for $\delta^{18}O$. (See Electronic Appendix 1 for age references.)

recycling of supracrustal rocks is demonstrated globally in a study of $\delta^{18}O$ of igneous zircon spanning most of Earth's magmatic history (Valley *et al.*, 2005), and increasing 'supracrustal oxygen' with time is seen during magmatic refinement of the Gondwana supercontinent (Kemp *et al.*, 2006) and Superior craton (Moser *et al.*, 2008). In the SNB, individual magmatic pulses generally record greater crustal recycling with time (Fig. 13), including the eastern Sierra where $\delta^{18}O$(Zrc) increases slightly. Some short-lived pulses (e.g. 103–102 Ma) are isotopically homogeneous, suggesting insufficient time for the onset of melting of crustal material. Overall, the SNB demonstrates that arcs may not record the same supracrustal oxygen increase as occurs during long-term crustal growth, but that such patterns are resolvable at the time-scale of individual magmatic episodes.

Evolution of the Sierran arc

We now integrate spatial and temporal patterns of SNB magma geochemistry and present a tectonic model in the form of a scheme portraying three critical times during construction of the batholith (Fig. 14).

Following the Nevadan Orogeny, the future Sierra was underlain by basement oceanic terranes accreted to North America and overlying sedimentary cover sequences (Fig. 14a). Subduction and underplating, or underthrusting in the Triassic and Jurassic probably contaminated the subarc lithospheric mantle. The eastern Sierra inherited Proterozoic North American crust and complementary lithospheric mantle, as shown by the $\delta^{18}O$ break recorded in Jurassic and Triassic plutons that stitch across the eastern Sierra Break (Fig. 14a), and the patterns of supracrustal contamination in these and Cretaceous plutons.

Subduction of the Farallon Plate initiated major magmatism by 120 Ma and produced significant batholith volume by 110 Ma (Figs 13a and 14b). Largely depleted mantle sources produced the plutons in the Foothills Zone, with minimal crustal interaction. The Fine Gold Suite, however, documents the onset of massive supracrustal recycling. Increased involvement of the wall-rocks of the Calaveras Complex, Kings Sequence, and cryptic contributions from altered ocean crust and Proterozoic rocks led to more complex isotopic signatures in magmas towards the PA/NA break.

The later stages of magmatism in the SNB highlight the role of tectonic reconfigurations in magma evolution. The deformation field of the Sierran arc is believed to have switched from contraction to transpression and dextral shearing because of changing convergence of the Farallon Plate in the late Cretaceous (Tobisch & Cruden, 1995; Tobisch *et al.*, 1995; Tikoff & de Saint Blanquat, 1997; Fig. 14c). Recent work on the proto-Kern Canyon fault shows evidence for intra-arc shortening at 95 Ma in response to this convergence switch (Nadin & Saleeby, 2008). Shortening potentially suppressed voluminous magmatism, as is seen in the lull at 95 Ma (Fig. 13b). However, post 95 Ma transpression established a positive feedback between magmatism and deformation, facilitating emplacement of the Sierra Crest magmas (Glazner, 1991; Tikoff & de Saint Blanquat, 1997). Shear-enhanced magma emplacement of eastern Sierra magmas possibly facilitated intrusion from MASH zone sources into the upper crust, thereby reducing crustal contamination. Likewise, transpressional conduits may have affected the constancy of $\delta^{18}O$ seen within some units. Homogeneous $\delta^{18}O$ in some plutons in the Tuolumne Suite emplaced over 2–3 Myr (Coleman *et al.*, 2004) favors enduring magma sources and conduits. Spatially variable $\delta^{18}O$ in plutons such as the Mount Givens indicates heterogeneous magmas, possibly the resulting of switching of sources (and conduits) during deformation, varying amounts of contamination, or magma mixing in evolving magma plumbing systems. In the southern Sierra, greater recycling of crustal rocks with time (Lackey *et al.*, 2005) corresponds to increased ductile deformation, including both vertical and lateral transport of wall-rocks in response to elevated

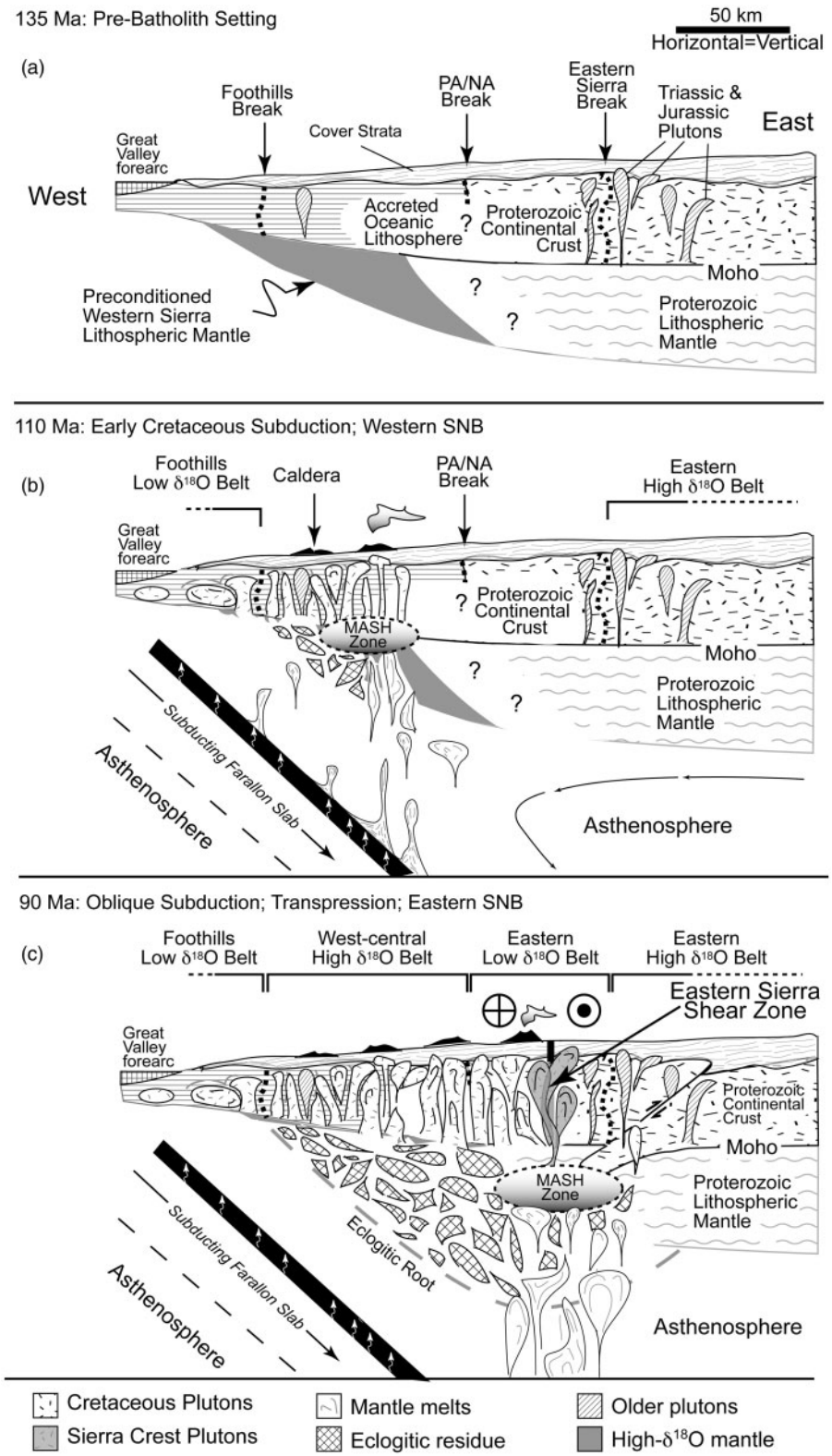

Fig. 14. Model for the origin of the distinct $\delta^{18}O$ belts of the central Sierra Nevada. (a) Early Cretaceous setting before voluminous magmatism, showing distinct basement and lithospheric mantle domains, overlying sediments, and older plutons. The Foothills and eastern Sierra crustal breaks are shown as trans-crustal; '?' symbols indicate uncertainty of the geometry and depth of the PA/NA break. The transition from oceanic to North American lithospheric mantle is also uncertain, although an east-dipping contact is inferred. (b) By 110 Ma, increased magmatism mobilized accreted supracrustal rocks into the western SNB high-$\delta^{18}O$ belt, inboard of the low-$\delta^{18}O$ belt. A relatively shallow western MASH zone resulted in widespread crustal melting. (c) At 90 Ma, transpression and increased rates of subduction facilitated emplacement of voluminous eastern SNB magmas from lithospheric mantle sources. Intra-arc shortening by lithospheric under-thrusting temporarily stifled magmatism, possibly inserting Proterozoic lower crust into the sub-arc mantle. 'Eclogitic root' refers to eclogitic residues expelled from the MASH zone. Transect line corresponds to Fig. 5.

geothermal gradients (Saleeby *et al.*, 2003). Thus, tectonic 're-shuffling' in the arc, such as downward flow of wall-rocks, or intra-arc thrusting (Fig. 14c), could possibly have rejuvenated magma sources with crustal rocks.

CONCLUDING REMARKS

The data presented in this study and by Lackey *et al.* (2005, 2006) put in place a modern and comprehensive oxygen isotope evaluation of the Sierra Nevada batholith. Values of $\delta^{18}O$(Zrc) provide clear records of changing magmatic $\delta^{18}O$ in the batholith, and calculation of $\delta^{18}O$(WR) values using zircon as a magmatic benchmark can be used to circumvent widespread resetting of the $\delta^{18}O$ of whole-rocks and single minerals such as quartz. Moreover, examples from the Barcroft pluton and Saddlebag Lake meta-rhyolite illustrate how $\delta^{18}O$ analysis of a refractory mineral such as zircon is a powerful means to deconvolve magmatic and metamorphic histories previously unobtainable from pervasively altered rocks.

Recognition of distinct belts of $\delta^{18}O$ values reveals both transverse and longitudinal domains within the batholith and a markedly more complex system than in the coeval Peninsular Ranges batholith. Large-scale pre-batholith boundaries resolved by $\delta^{18}O$ mapping better define the locations of previously inferred terrane boundaries, including cryptic boundaries such as the Foothills Break. Furthermore, the pre-batholith arrangement of basement and supracrustal rocks, structural reconfiguration during the evolution of the batholith, and different magma source depths, led to the overall patterns of $\delta^{18}O$. Lastly, the discrete magma systems that we resolve at different scales in time and space, from batholith to pluton scale, emphasizes the dynamic nature of the Sierran arc.

ACKNOWLEDGEMENTS

All isotope analyses were completed by J.S.L. in the University of Wisconsin Stable Isotope Laboratory with support from DOE 93ER14389 and NSF EAR99-02973 and EAR02-07340. A UW Dean Morgridge Distinguished Graduate Fellowship, GSA and Sigma Xi grants, and the UW Department of Geology and Geophysics Weeks Fund supported portions of this work. Pomona College Geology Department faculty research funds provided valuable support for publication of this study. We thank Mike Spicuzza for assistance with stable isotope analysis, Brian Hess for making thin sections and grain mounts, and Clark Johnson and Brian Beard for the use of the rock crushing and mineral separation laboratories. Clark Johnson, Brad Singer, Elizabeth King, William Peck, Ilya Bindeman, Cory Clechenko, Aaron Cavosie, and Tom Lapen have added valuable discussion of portions of this research. We thank Martha House for many of the samples. Jason Saleeby, Kent Ratajeski, and Basil Tikoff are thanked for their helpful discussions and samples. Drew Coleman, Rich Gaschnig, and John Gracely, at UNC, kindly provided unpublished U–Pb ages and helpful discussions of the geochronology of the eastern Sierra. Ron Kistler graciously shared unpublished isotope data. Hans Hinke assisted in the field. David Graber and Jan van Wagtendonk helped us obtain permits to sample in Sequoia, Kings Canyon, and Yosemite National Parks. Detailed and encouraging reviews by Allen Glazner, Tom Sisson, Ron Frost, and Charlotte Allen helped improve this paper.

SUPPLEMENTARY DATA

Supplementary data for this paper are available at *Journal of Petrology* online.

REFERENCES

Ague, J. J. (1997). Thermodynamic calculation of emplacement pressures for batholithic rocks, California: Implications for the aluminum-in-hornblende barometer. *Geology* **25**, 563–566.

Ague, J. J. & Brimhall, G. H. (1988*a*). Magmatic arc asymmetry and distribution of anomalous plutonic belts in the batholiths of California: effects of assimilation, crustal thickness, and depth of crystallization. *Geological Society of America Bulletin* **100**, 912–927.

Ague, J. J. & Brimhall, G. H. (1988*b*). Regional variations in bulk chemistry, mineralogy, and the compositions of mafic and accessory minerals in the batholiths of California: with Suppl. Data 88–13. *Geological Society of America Bulletin* **100**, 891–911.

Annen, C., Blundy, J. D. & Sparks, R. S. J. (2006). The genesis of intermediate and silicic magmas in deep crustal hot zones. *Journal of Petrology* **47**, 505–539.

Appora, I., Eiler, J. M., Matthews, A. & Stolper, E. M. (2003). Experimental determination of oxygen isotope fractionations between CO_2 vapor and soda-melilite melt. *Geochimica et Cosmochimica Acta* **67**, 459–471.

Bateman, P. C. (1992). Plutonism in the central part of the Sierra Nevada Batholith, California. *US Geological Survey, Professional Papers* **1483**, pp. 1–186.

Bateman, P. C. & Chappell, B. W. (1979). Crystallization, fractionation, and solidification of the Tuolumne Intrusive Series, Yosemite National Park, California. *Geological Society of America Bulletin* **90**, 465–482.

Bateman, P. C., Dodge, F. C. W. & Kistler, R. W. (1991). Magnetic susceptibility and relation to initial $^{87}Sr/^{86}Sr$ for granitoids of the central Sierra Nevada, California. *Journal of Geophysical Research, B, Solid Earth and Planets* **96**, 19555–19568.

Bindeman, I. N. & Valley, J. W. (2002). Oxygen isotope study of the Long Valley magma system, California: isotope thermometry and convection in large silicic magma bodies. *Contributions to Mineralogy and Petrology* **144**, 185–205.

Böhlke, J. K. & Kistler, R. W. (1986). Rb–Sr, K–Ar, and stable isotope evidence for the ages and sources of fluid components of gold-bearing quartz veins in the northern Sierra Nevada foothills metamorphic belt, California. *Economic Geology* **81**, 296–322.

Chacko, T., Cole, D. R. & Horita, J. (2001). Equilibrium oxygen, hydrogen, and carbon isotope fractionation factors applicable to geological systems. In: Valley, J. W. & Cole, D. R. (eds) *Stable Isotope Geochemistry. Mineralogical Society of America/Geochemical Society, Reviews in Mineralogy and Geochemistry* **43**, 1–81.

Chen, J. H. & Moore, J. G. (1979). Late Jurassic Independence dike swarm in eastern California. *Geology* **7**, 129–133.

Chen, J. H. & Moore, J. G. (1982). Uranium–lead isotopic ages from the Sierra Nevada batholith, California. *Journal of Geophysical Research B* **87**, 4761–4784.

Chen, J. H. & Tilton, G. R. (1991). Applications of lead and strontium isotopic relationships to the petrogenesis of granitoid rocks, central Sierra Nevada batholith, California. *Geological Society of America Bulletin* **103**, 437–447.

Clayton, R. N., Goldsmith, J. R. & Mayeda, T. K. (1989). Oxygen isotope fractionation in quartz, albite, anorthite and calcite. *Geochimica et Cosmochimica Acta* **53**, 725–733.

Clemens-Knott, D. (1992). Geologic and isotopic investigations of the Early Cretaceous Sierra Nevada batholith, Tulare County, California, and the Ivrea Zone, Northwest Italian Alps: examples of interaction between mantle-derived magma and continental crust. Ph.D. thesis, California Institute of Technology, Pasadena.

Coleman, D. S. & Glazner, A. F. (1997). The Sierra Crest magmatic event: rapid formation of juvenile crust during the Late Cretaceous in California. *International Geology Review* **39**, 768–787.

Coleman, D. S., Frost, T. P. & Glazner, A. F. (1992). Evidence from the Lamarck Granodiorite for rapid Late Cretaceous crust formation in California. *Science* **258**, 1924–1926.

Coleman, D. S., Gray, W. & Glazner, A. F. (2004). Rethinking the emplacement and evolution of zoned plutons: geochronologic evidence for incremental assembly of the Tuolumne Intrusive Suite, California. *Geology* **32**, 433–436.

Couglan, R. A. N. (1990). Studies in diffusional transport: Grain boundary transport of O in feldspars, diffusion of O, strontium, and the REEs in garnet and thermal histories of granitic intrusions in south–central Maine using O isotopes. Ph.D. thesis, Brown University, Providence, RI.

DePaolo, D. J. (1980). Sources of continental crust: neodymium isotope evidence from the Sierra Nevada and Peninsular Ranges. *Science* **209**, 684–687.

DePaolo, D. J. (1981). A neodymium and strontium isotopic study of the Mesozoic calc-alkaline granitic batholiths of the Sierra Nevada and Peninsular Ranges, California. *Journal of Geophysical Research B* **86**, 10470–10488.

Dodson, M. H. (1973). Closure temperature in cooling geochronological and petrologic systems. *Contributions to Mineralogy and Petrology* **40**, 259–274.

Doe, B. R. & Delevaux, M. H. (1973). Variations in lead-isotopic compositions in Mesozoic granitic rocks of California: a preliminary investigation. *Geological Society of America Bulletin* **84**, 3513–3526.

Ducea, M. N. (1998). A petrologic investigation of deep-crustal and upper-mantle xenoliths from the Sierra Nevada, California: constraints on lithospheric composition beneath continental arcs and the origin of Cordilleran batholiths. Ph.D. thesis, California Institute of Technology, Pasadena.

Ducea, M. N. (2001). The California Arc: thick granitic batholiths, eclogitic residues, lithospheric-scale thrusting, and magmatic flare-ups. *GSA Today* **11**, 4–10.

Ducea, M. N. (2002). Constraints on the bulk composition and root foundering rates of continental arcs: a California arc perspective. *Journal of Geophysical Research, B, Solid Earth and Planets* **107**, ECV 15.1–15.13.

Ernst, W. G. & Rumble, D., III (2003). Oxygen isotopic study of late Mesozoic cooling of the Mount Barcroft area, central White Mountains, eastern California. *Contributions to Mineralogy and Petrology* **144**, 639–651.

Ernst, W. G., Coleman, D. S. & Van de Ven, C. M. (2003). Petrochemistry of granitic rocks in the Mount Barcroft area: implications for arc evolution, central White Mountains, easternmost California. *Geological Society of America Bulletin* **115**, 499–512.

Farver, J. R. & Yund, R. A. (1991). Oxygen diffusion in quartz: dependence on temperature and water fugacity. *Chemical Geology* **90**, 55–70.

Fliedner, M. M., Klemperer, S. L. & Christensen, N. I. (2000). Three-dimensional seismic model of the Sierra Nevada Arc, California, and its implications for crustal and upper mantle composition. *Journal of Geophysical Research, B, Solid Earth and Planets* **105**, 10899–10921.

Fu, B., Page, F. Z., Cavosie, A. J., Fournelle, J. H., Kita, N. T., Lackey, J. S., Wilde, S. A. & Valley, J. W. (2008). Ti-in-zircon thermometry: applications and limitation. *Contributions to Mineralogy and Petrology* doi:10.1007/s00410-008-0281-5.

Garlick, G. D. (1966). Oxygen isotope fractionation in igneous rocks. *Earth and Planetary Science Letters* **1**, 361–368.

Gaschnig, R. M., Coleman, D. S. & Glazner, A. F. (2006). Twin of the Tuolumne: new geochronology from the Mono Pass intrusive suite. *Geological Society of America, Abstracts with Programs* **38**, 559.

Glazner, A. F. (1991). Plutonism, oblique subduction, and continental growth: an example from the Mesozoic of California. *Geology* **19**, 784–786.

Godfrey, J. D. (1962). The deuterium content of hydrous minerals from the east–central Sierra Nevada and Yosemite National Park. *Geochimica et Cosmochimica Acta* **26**, 1215–1245.

Gromet, P. L. & Silver, L. T. (1987). REE variations across the Peninsular Ranges batholith: implications for batholithic petrogenesis and crustal growth in magmatic arcs. *Journal of Petrology* **28**, 75–125.

Hildreth, W. & Moorbath, S. (1988). Crustal contributions to arc magmatism in the Andes of central Chile. *Contributions to Mineralogy and Petrology* **98**, 455–489.

Hill, M., O'Neil, J. R., Noyes, H., Frey, F. A. & Wones, D. R. (1988). Sr, Nd, and O isotope variations in compsitionally zoned and unzoned plutons in the central Sierra Nevada batholith. *American Journal of Science* **288-A**, 213–214.

House, M. A., Wernicke, B. P., Farley, K. A. & Dumitru, T. A. (1997). Cenozoic thermal evolution of the central Sierra Nevada, California, from (U–Th)/He thermochronometry. *Earth and Planetary Science Letters* **151**, 167–179.

House, M. A., Wernicke, B. P. & Farley, K. A. (1998). Dating topography of the Sierra Nevada, California, using apatite (U–Th)/He ages. *Nature* **396**, 66–69.

House, M. A., Wernicke, B. P. & Farley, K. A. (2001). Paleogeomorphology of the Sierra Nevada, California, from (U–Th)/He ages in apatite. *American Journal of Science* **301**, 77–102.

Jennings, C. W., Strand, R. G. & Rogers, T. H. (1977). *Geologic map of California*. California Division of Mines and Geology, Washington, DC: Williams and Heintz Map Corporation, 1 sheet, 1:750 000.

Kemp, A. I. S., Hawkesworth, C. J., Paterson, B. A. & Kinny, P. D. (2006). Episodic growth of the Gondwana supercontinent from hafnium and oxygen isotopes in zircon. *Nature* **439**, 580–583.

King, E. M. & Valley, J. W. (2001). The source, magmatic contamination, and alteration of the Idaho batholith. *Contributions to Mineralogy and Petrology* **142**, 72–88.

Kistler, R. W. (1990). Two different lithosphere types in the Sierra Nevada, California. In: Anderson, L. (ed.) *The Nature and Origin of Cordilleran Magmatism. Geological Society of America, Memoirs* **174**, 271–281.

Kistler, R. W. (1993). Mesozoic Intrabatholithic faulting, Sierra Nevada, California. In: Dunne, G. & McDougall, K. (eds) *Mesozoic Paleography of the Western United States II*. Los Angeles: Pacific Section, SEPM, pp. 247–262.

Kistler, R. W. & Fleck, R. J. (1994). Field guide for a transect of the central Sierra Nevada, California: geochronology and isotope geology. *US Geological Survey, Open-File Report* **94-0267**, 50 pp.

Kistler, R. W. & Peterman, Z. E. (1973). Variations in Sr, Rb, K, Na, and initial Sr^{87}/Sr^{86} in Mesozoic granitic rocks and intruded wall rocks in central California. *Geological Society of America Bulletin* **84**, 3489–3512.

Kistler, R. W. & Peterman, Z. E. (1978). Reconstruction of crustal blocks of California on the basis of initial strontium isotopic compositions of Mesozoic granitic rocks. *US Geological Survey, Professional Papers* **1071**, 17 pp.

Kistler, R. W. & Ross, D. C. (1990). A strontium isotopic study of plutons and associated rocks of the southern Sierra Nevada and vicinity, California. *US Geological Survey Bulletin* **1920**, 20 pp.

Kistler, R. W., Chappell, B. W., Peck, D. L. & Bateman, P. C. (1986). Isotopic variation in the Tuolumne intrusive suite, central Sierra Nevada, California. *Contributions to Mineralogy and Petrology* **94**, 205–220.

Kohn, M. J. & Valley, J. W. (1998). Effects of cation substitutions in garnet and pyroxene on equilibrium oxygen isotope fractionations. *Journal of Metamorphic Geology* **16**, 625–639.

Kylander-Clark, A. R. C., Coleman, D. S., Glazner, A. F. & Bartley, J. M. (2005). Evidence for 65 km of dextral slip across Owens Valley, California, since 83 Ma. *Geological Society of America Bulletin* **117**, 962–968.

Lackey, J. S. (2005). The magmatic and alteration history of the Sierra Nevada batholith as recorded by oxygen isotope ratios in zircon, titanite, garnet, and quartz. PhD thesis, University of Wisconsin, Madison.

Lackey, J. S., Valley, J. W. & Chen, J. H. (2001). Correlated O–Sr–Pb isotope ratios in the West–Central Sierra Nevada batholith, California. *Geological Society of America, Abstracts with Programs* **33**, 295.

Lackey, J. S., Valley, J. W., Stockli, D. F. & House, M. A. (2003). Magmatic processes in the central Sierra Nevada batholith: a cryptic pre-Jurassic boundary in Long Valley, California. *Geological Society of America, Abstracts with Programs* **35**, 92.

Lackey, J. S., Valley, J. W. & Saleeby, J. B. (2005). Supracrustal input to magmas in the deep crust of Sierra Nevada batholith: evidence from high-$\delta^{18}O$ zircon. *Earth and Planetary Science Letters* **235**, 315–330.

Lackey, J. S., Valley, J. W. & Hinke, H. J. (2006). Deciphering the source and contamination history of peraluminous magmas using $\delta^{18}O$ of accessory minerals: examples from garnet-bearing granitoids of the Sierra Nevada batholith. *Contributions to Mineralogy and Petrology* **151**, 20–44.

Lee, C. T., Yin, Q., Rudnick, R. L., Chesley, J. T. & Jacobsen, S. B. (2000). Osmium isotopic evidence for Mesozoic removal of lithospheric mantle beneath the Sierra Nevada, California. *Science* **289**, 1912–1916.

Lee, C.-T., Morton, D. M., Kistler, R. W. & Baird, A. K. (2007). Petrology and tectonics of Phanerozoic continent formation: from island arcs to accretion and continental arc magmatism. *Earth and Planetary Science Letters* **263**, 370–387.

Magaritz, M. & Taylor, H. P., Jrs (1976). Oxygen, hydrogen and carbon isotope studies of the Franciscan Formation, Coast Ranges, California. *Geochimica et Cosmochimica Acta* **40**, 215–234.

Masi, U., O'Neil, J. R. & Kistler, R. W. (1981). Stable isotope systematics in Mesozoic granites of central and northern California and southwestern Oregon. *Contributions to Mineralogy and Petrology* **76**, 116–126.

McCulloch, M. T., Gregory, R. T., Wasserburg, G. J. & Taylor, H. P. (1980). A neodymium, strontium, and oxygen isotope study of the Cretaceous Samail Ophiolite and implications for the petrogenesis and seawater–hydrothermal alteration of oceanic crust. *Earth and Planetary Science Letters* **46**, 201–211.

McNulty, B. A., Tobisch, O. T., Cruden, A. R. & Gilder, S. (2000). Multi-stage emplacement of the Mt. Givens pluton, central Sierra Nevada, California,. *Geological Society of America Bulletin* **112**, 103–119.

Montel, J. M. & Vielzeuf, D. (1997). Partial melting of metagreywackes. 2. Compositions of minerals and melts. *Contributions to Mineralogy and Petrology* **128**, 176–196.

Moore, J. G. (1959). The quartz diorite boundary line in the western United States. *Journal of Geology* **67**, 198–210.

Moore, J. G. (2000). *Exploring the Highest Sierra*. Palo Alto, CA: Stanford University Press, 427 pp.

Moore, J. G. & Sisson, T. W. (1987). Preliminary geologic map of Sequoia and Kings Canyon national parks, California. *US Geological Survey, Open-File Report* **87-0651**, 1 Sheet, 1:250 000.

Moser, D. E., Bowman, J. R., Wooden, J. L., Valley, J. W., Mazdab, F. & Kita, N. (2008). Creation of a continent recorded in zircon zoning. *Geology* **36**, 239–242.

Muehlenbachs, K. (1998). The oxygen isotopic composition of the oceans, sediments and the seafloor. *Chemical Geology* **145**, 263–273.

Mukhopadhyay, B. & Manton, W. I. (1994). Upper-mantle fragments from beneath the Sierra Nevada Batholith: partial fusion, fractional crystallization, and metasomatism in a subduction-related ancient lithosphere. *Journal of Petrology* **35**, 1417–1450.

Nadin, E. S. & Saleeby, J. B. (2008). Disruption of regional primary structure of the Sierra Nevada batholith by the Kern Canyon fault system, California. *Geological Society of America, Special Papers* **438**, 429–454.

Page, F. Z., Ushikubo, T., Kita, N. T., Riciputi, L. R. & Valley, J. W. (2007). High-precision oxygen isotope analysis of picogram samples reveals 2 μm gradients and slow diffusion in zircon. *American Mineralogist* **92**, 1772–1775.

Peck, W. H., Valley, J. W., Corriveau, L., Davidson, A., McLelland, J. & Farber, D. A. (2004). Oxygen-isotope constraints on terrane boundaries and origin of 1·18–1·13 Ga granitoids in the southern Grenville Province. *Geological Society of America, Memoirs* **197**, 163–183.

Ratajeski, K., Glazner, A. F. & Miller, B. V. (2001). Geology and geochemistry of mafic to felsic plutonic rocks in the Cretaceous intrusive suite of Yosemite Valley, California. *Geological Society of America Bulletin* **113**, 1486–1502.

Ratajeski, K., Glazner, A. F. & Sisson, T. W. (2005). Experimental and geochemical evidence for derivation of the El Capitan Granite, California, by partial melting of hydrous gabbroic lower crust. *Contributions to Mineralogy and Petrology* **149**, 713–734.

Robinson, A. C. & Kistler, R. W. (1986). Maps showing isotopic dating in the Walker Lake 1 degrees by 2 degrees Quadrangle, California and Nevada. *US Geological Survey, Miscellaneous Field Studies Map MF-1382-N*, 49, 3 sheets, 1:250 000.

Ross, D. C. (1983*a*). Generalized geologic map of the southern Sierra Nevada, California, showing the location of basement samples for which whole rock ^{18}O has been determined. *US Geological Survey, Open-File Report* **83-0904**, 1 sheet, 1:250 000.

Ross, D. C. (1983*b*). Generalized geologic map of the southern Sierra Nevada, California, showing the location of samples for which K–Ar radiometric age data and Rb/Sr data have been determined. *US Geological Survey, Open-File Report* **83-0231**, 1 sheet, 1:250 000.

Ross, D. C. (1987). Generalized geologic map of the basement rocks of the southern Sierra Nevada, California. *US Geological Survey, Open-File Report* **87-0276**, 30 pp.

Saleeby, J. B. (1992). Petrotectonic and paleogeographic settings of U.S. Cordilleran ophiolites. In: Burchfiel, B. C., Lipman, P. W. &

Zoback, M. L. (eds) *The Cordilleran Orogen: Conterminous US: The Geology of North America*. Boulder, CA: Geological Society of America. pp. 653–682.

Saleeby, J. B. & Busby, C. (1993). Paleogeographic and tectonic setting of axial and western metamorphic framework rocks of the southern Sierra Nevada, California. In: Dunne, G. C. & McDougall, K. (eds) *Mesozoic Paleogeography of the Western United States: II*. Los Angeles, CA: Pacific Section 71, SEPM, pp. 197–225.

Saleeby, J. B., Speed, R. C., Blake, M. C., Allmendinger, R. W., Gans, P. B., Kistler, R. W., Ross, D. C., Stauber, D. A., Zoback, M. L., Griscom, A. & McCulloch, D. S. (1986). *Centennial Continent/Ocean Transect 10, Corridor C-2: Central California offshore to the Colorado Plateau*. Boulder, CA: Geological Society of America, 63 pp., 2 sheets, 1:500 000.

Saleeby, J. B., Sams, D. B. & Kistler, R. W. (1987). U/Pb zircon, strontium, and oxygen isotopic and geochronological study of the southernmost Sierra Nevada Batholith, California. *Journal of Geophysical Research, B, Solid Earth and Planets* **92**, 10443–10466.

Saleeby, J., Ducea, M. & Clemens Knott, D. (2003). Production and loss of high-density batholithic root, southern Sierra Nevada, California. *Tectonics* **22**, doi:10.1029/2002TC001374.

Scoates, J. S. & Frost, C. D. (1996). A strontium and neodymium isotopic investigation of the Laramie anorthosites, Wyoming, USA: Implications for magma chamber processes and the evolution of magma conduits in Proterozoic anorthosites. *Geochimica et Cosmochimica Acta* **60**, 95–107.

Sharp, Z. D., Giletti, B. J. & Yoder, H. S., Jr (1991). Oxygen diffusion rates in quartz exchanged with CO_2. *Earth and Planetary Science Letters* **107**, 339–348.

Silver, L. T., Taylor, H. P., Jr & Chappell, B. (1979). Some petrological, geochemical and geochronological observations of the Peninsular Ranges Batholith near the international border of the U.S.A. and Mexico. In: Abbott, P. L. & Todd, V. (eds) *Mesozoic Crystalline Rocks: Peninsular Ranges Batholith and Pegmatites, Point Sal Ophiolite*. San Diego, CA: San Diego State University, pp. 83–110.

Sisson, T. W., Grove, T. L. & Coleman, D. S. (1996). Hornblende gabbro sill complex at Onion Valley, California, and a mixing origin for the Sierra Nevada Batholith. *Contributions to Mineralogy and Petrology* **126**, 81–108.

Sisson, T. W., Ratajeski, K., Hankins, W. B. & Glazner, A. F. (2005). Voluminous granitic magmas from common basaltic sources. *Contributions to Mineralogy and Petrology* **148**, 635–661.

Snow, C. A. & Scherer, H. H. (2006). Terranes of the western Sierra Nevada Foothills metamorphic belt, California: A critical review. *International Geology Review* **48**, 46–62.

Spicuzza, M. J., Valley, J. W. & McConnell, V. S. (1998). Oxygen isotope analysis of whole rock via laser fluorination: An air-lock approach. *Geological Society of America, Abstracts with Programs* **30**, 80.

Stern, T. W., Bateman, P. C., Morgan, B. A., Newell, M. F. & Peck, D. L. (1981). Isotopic U–Pb ages of zircon from the granitoids of the central Sierra Nevada, California. *US Geological Survey, Professional Papers* **1185**, 17 pp.

Stevens, C. H., Stone, P., Dunne, G. C., Greene, D. C., Walker, J. D. & Swanson, B. J. (1997). Paleozoic and Mesozoic evolution of east–central California. *International Geology Review* **39**, 788–829.

Stockli, D. F., Dumitru, T. A., McWilliams, M. O. & Farley, K. A. (2003). Cenozoic Tectonic Evolution of the White Mountains, California and Nevada. *Geological Society of America Bulletin* **115**, 788–816.

Taylor, H. P. & Sheppard, S. M. F. (1986). Igneous rocks: I. Processes of isotopic fractionation and isotope systematics. In: Valley, J. W., Taylor, H. P., Jr & O'Neil, J. R. (eds) *Stable Isotopes in High Temperature Geological Processes. Mineralogical Society of America, Reviews in Mineralogy* **16**, 227–271.

Taylor, H. P. & Silver, L. T. (1978). Oxygen isotope relationships in plutonic igneous rocks of the Peninsular Ranges Batholith, southern and Baja California. *US Geological Survey, Open-File Report* **78-0701**, 423–426.

Tikoff, B. & de Saint Blanquat, M. (1997). Transpressional shearing and strike-slip partitioning in the Late Cretaceous Sierra Nevada magmatic arc, California. *Tectonics* **16**, 442–459.

Tobisch, O. T. & Cruden, A. R. (1995). Fracture-controlled magma conduits in an obliquely convergent continental magmatic arc. *Geology* **23**, 941–944.

Tobisch, O. T., Saleeby, J. B., Renne, P. R., McNulty, B. A. & Tong, W. (1995). Variations in deformation fields during development of a large-volume magmatic arc, central Sierra Nevada, California. *Geological Society of America Bulletin* **107**, 148–166.

Truschel, J. P. (1996). Petrogenesis of the Fine Gold intrusive suite, Sierra Nevada Batholith, California. M.S. thesis, California State University, Northridge, California.

Tulloch, A. J. & Kimbrough, D. L. (2003). Paired plutonic belts in convergent margins and the development of high Sr/Y magmatism: Peninsular Ranges Batholith of Baja California and Median Batholith of New Zealand. *Geological Society of America, Special Papers* **374**, 275–295.

Valley, J. W. (2003). Oxygen isotopes in zircon. In: Hanchar, J. M. & Hoskin, P. W. O. (eds) *Zircon. Mineralogical Society of America/Geochemical Society, Reviews in Mineralogy and Geochemistry* **53**, 343–385.

Valley, J. W., Chiarenzelli, J. R. & McLelland, J. M. (1994). Oxygen isotope geochemistry of zircon. *Earth and Planetary Science Letters* **126**, 187–206.

Valley, J. W., Kitchen, N., Kohn, M. J., Niendorf, C. R. & Spicuzza, M. J. (1995). UWG-2, a garnet standard for oxygen isotope ratios: strategies for high precision and accuracy with laser heating. *Geochimica et Cosmochimica Acta* **59**, 5223–5231.

Valley, J. W., Kinny, P. D., Schulze, D. J. & Spicuzza, M. J. (1998). Zircon megacrysts from kimberlite: oxygen isotope variability among mantle melts. *Contributions to Mineralogy and Petrology* **133**, 1–11.

Valley, J. W., Bindeman, I. N. & Peck, W. H. (2003). Empirical calibration of oxygen isotope fractionation in zircon. *Geochimica et Cosmochimica Acta* **67**, 3257–3266.

Valley, J. W., Lackey, J. S., Cavosie, A. J., Clechenko, C., Spicuzza, M. J., Basei, M. A. S., Bindeman, I. N., Ferreira, V. P., Sial, A. N., King, E. M., Peck, W. H., Sinha, A. K. & Wei, C. S. (2005). 4·4 billion years of crustal maturation from oxygen isotope ratios of zircon. *Contributions to Mineralogy and Petrology* **150**, 561–580.

Vielzeuf, D. & Schmidt, M. W. (2001). Melting relations in hydrous systems revisited: application to metapelites, metagreywackes and metabasalts. *Contributions to Mineralogy and Petrology* **141**, 251–267.

Vielzeuf, D., Veschambre, M. & Brunet, F. (2005). Oxygen isotope heterogeneities and diffusional profiles in composite metamorphic/magmatic garnets from the Pyrenees. *American Mineralogist* **90**, 463–472.

Wenner, J. M. & Coleman, D. S. (2004). Magma mixing and Cretaceous crustal growth: geology and geochemistry of granites in the central Sierra Nevada batholith, California. *International Geology Review* **46**, 880–903.

Zeng, L., Ducea, M. & Saleeby, J. B. (2005). Geochemical characteristics of crustal anatexis during the formation of migmatite at the southern Sierra Nevada, California. *Contributions to Mineralogy and Petrology* **150**, 386–402.

Zhao, Z. & Zheng, Y. (2003). Calculation of oxygen isotope fractionation in magmatic rocks. *Chemical Geology* **193**, 59–80.